Array Design for Angle of Arrival Estimation using the Worst-Case Two-Target Cramér-Rao Bound

Kokke, Costas A.; Coutino, Mario; Heusdens, Richard; Leus, Geert

DOI
10.1109/OJSP.2025.3558686

Publication date
2025

Document Version
Final published version

Published in
IEEE Open Journal of Signal Processing

IEEE Open Journal of Signal Processing

Received 7 October 2024; revised 11 February 2025; accepted 27 March 2025. Date of publication 7 April 2025; date of current version 25 April 2025. The review of this article was arranged by Associate Editor Elias Aboutanios.

Digital Object Identifier 10.1109/OJSP.2025.3558686

Array Design for Angle of Arrival Estimation Using the Worst-Case Two-Target Cramér-Rao Bound

COSTAS A. KOKKE [1] (Graduate Student Member, IEEE), MARIO COUTINO [2] (Member, IEEE), RICHARD HEUSDENS [3] (Senior Member, IEEE), AND GEERT LEUS [1] (Fellow, IEEE)

[1]Faculty of Electrical Engineering, Mathematics, and Computer Science, Delft University of Technology, 2628 CD Delft, The Netherlands
[2]Acoustics and Sonar Department, Netherlands Organisation for Applied Scientific Research, 2509 JG The Hague, The Netherlands
[3]Faculty of Military Sciences, Netherlands Defence Academy, 1781 AC Den Helder, The Netherlands

CORRESPONDING AUTHOR: COSTAS A. KOKKE (email: c.a.kokke@tudelft.nl).

An earlier version of this paper was presented in part at the 2023 IEEE International Conference on Acoustics, Speech and Signal Processing [DOI: 10.1109/ICASSP49357.2023.10094942], and the 2023 57th Asilomar Conference on Signals, Systems, and Computers [DOI: 10.1109/IEEECONF59524.2023.10476966].

This work was supported by the Netherlands Organisation for Applied Scientific Research (TNO) and the Netherlands Defence Academy (NLDA).

ABSTRACT Sparse array design is used to help reduce computational, hardware, and power requirements compared to uniform arrays while maintaining acceptable performance. Although minimizing the Cramér-Rao bound has been adopted previously for sparse sensing, it did not consider multiple targets and unknown target directions. To handle the unknown target directions when optimizing the Cramér-Rao bound, we propose to use the worst-case Cramér-Rao bound of two uncorrelated equal power sources with arbitrary angles. This new worst-case two-target Cramér-Rao bound metric has some resemblance to the peak sidelobe level metric which is commonly used in unknown multi-target scenarios. We cast the sensor selection problem for 3-D arrays using the worst-case two-target Cramér-Rao bound as a convex semi-definite program and obtain the binary selection by randomized rounding. We illustrate the proposed method through numerical examples, comparing it to solutions obtained by minimizing the single-target Cramér-Rao bound, minimizing the Cramér-Rao bound for known target angles, the concentric rectangular array and the boundary array. We show that our method selects a combination of edge and center elements, which contrasts with solutions obtained by minimizing the single-target Cramér-Rao bound. The proposed selections also exhibit lower peak sidelobe levels without the need for sidelobe level constraints.

INDEX TERMS Array processing, Cramer-Rao bound, multi-target estimation, sensor selection, sparse sensing.

I. INTRODUCTION

One of the primary functions of a radar system is angle of arrival estimation. To perform this task, modern radar employs antenna arrays to obtain spatially diverse data. The largest distance between elements in the array, also referred to as the array aperture, is the primary contributor to angular resolution. On the other hand, the density of the array, i.e., the small distances within the array, contributes to the prevention of spatial aliasing and the suppression of target interference. As such, it is desirable to have a large and densely populated array.

A large and dense array comes with a cost, though. Firstly, a large and dense array implies that many individual antennas are required to realize the array. While antennas themselves can be relatively cheap, especially in higher frequency bands, they do take up physical space. Furthermore, each antenna requires an RF frontend, and those are typically more expensive to design and acquire than antennas [1], [2], [3]. Each frontend comes with a power cost when in use, and when the array is dense, the power dissipation becomes another challenge. Additionally, when antennas are placed close together, particularly transmitters, there will be mutual coupling, which

is inversely proportional to the distance between the array elements [4], [5], [6], [7]. Suppose these challenges can be overcome, we are still left with the challenge of transferring all the acquired data and processing all the data within a meaningful timeframe. Both of these data challenges also increase the power requirements and cost of the total system.

While the previous list of challenges is likely by no means exhaustive, it should convince the reader that investigating array design to compromise on a maximally large and dense array is required in the design of modern radar systems. One such approach in array design is sensor selection. In sensor selection, one starts with a candidate array of (virtual) antennas with fixed positions and then selects the antennas from this candidate set to optimize a specified cost function. This approach is equivalent to grid-based sensor placement.

There are two main ways to think about sensor selection: offline and online. In offline sensor selection, the optimal selection is determined while the array is not in use. For example, the optimal sensor selection, or sensor placement, is computed during the design of the radar system. In this case, the candidate array of antennas need not physically exist. We simply optimize the selection and the physical system is realized based on this optimal selection. In this case, the time it takes to find the optimal array is less critical. During the design phase, it is not unreasonable to assume that the optimization of the sensor selection can be offloaded to a powerful computing system, and that it is acceptable to wait for some time for the optimum to be obtained.

Contrastingly, in online sensor selection, the optimization is done while the radar system is being operated. For example, if the cost function of the sensor selection depends on the environment, the optimal selection may change with changes in the environment and the optimization should be done repeatedly. Online sensor selection can also be used in the event of RF frontend failures if the antennas are switchable (switches are in place to change which frontends are connected to which antennas). Once a frontend fails, the sensor selection can be optimized again for the new number of useable frontends, ensuring that the performance degradation from the frontend failure is minimized. Multitask arrays, where part of the array may be used for other tasks such as communications, may also benefit from adaptively performing sensor selection. In all these cases, it is important that the sensor selection can be performed in a reasonable time on limited hardware.

The sensor selection problem for direction of arrival (DoA) estimation exists in more applications than just radar, of course. For example, DoA estimation can be used in emitter localization, which is of interest in localization using signals of opportunity [8]. In such cases, the motivation for using the two types of sensor selection described above also applies. So while in this work radar is considered as the example application, please note that what is discussed is largely applicable to DoA estimation using receiver arrays in general.

In the following, we highlight some previous work dealing with sensor selection, as well as some other approaches to array design. We will also discuss some works that have proposed metrics by which we can evaluate the performance of array designs.

A. PREVIOUS WORK

Sparse array design has received considerable attention for some decades now, using different design criteria. For example, the concept of minimum redundancy arrays (MRAs) is that a sparse array should have a minimal number of repeated inter-element spacings [9]. It has been shown that MRAs maximize resolution for a fixed number of sensors. A special case of the MRA is, of course, the zero-redundancy array, but it has been shown that such arrays only exist for small numbers of elements [10]. The MRA for a given number of elements, or a given candidate set of positions, is rather challenging to find however, and so approximations have been proposed, such as the low-redundancy linear arrays (LRLAs) [11] and concentric rectangular array (CRA) [7]. LRLAs are essentially a concession on MRAs, given that MRAs are difficult to design and typically found through exhaustive methods [7], [12]. LRLA design techniques such as [11], [13] are based on non-convex optimization methods and, as such, may not have a global optimality guarantee. Another example, the CRA, requires no optimization at all, and is shown to be the MRA for some specific square candidate uniform planar array (UPA) configurations. In these cases, the amount of sensors used is exactly the same as that of the boundary array (BA) [14], [15], [16], a simple sparse array design method where only the sensors on the boundary of the candidate set are chosen. For a UPA candidate set, this is of course far from an MRA, since it is essentially the combination of a few uniform linear arrays (ULAs). In contrast, the goal of the CRA in particular is to reduce the redundancy of the small inter-element distances since these have the most significant contribution to the mutual coupling problem. The nested [17], [18] and the co-prime arrays [19], [20] are other examples of sparse arrays that are designed by evaluating the inter-element spacing. Procedures exist to find them in 1-D and 2-D. Like the CRA, the motivation for these sparse arrays is not just reduced elements and/or RF frontends, but also reduced mutual coupling, particularly for the co-prime array. While these arrays are largely designed with the goal of target identifiability with fewer sensors than a ULA or UPA, [21] shows that such sparse arrays, in particular the nested array, can provide a better single-target Cramér-Rao Bound (CRB) than a ULA of the same number of sensors. Additionally, a CRB to specifically analyze sparse arrays such as MRAs, nested arrays and co-prime arrays, which are capable of identifying more targets than the number of sensors has been presented in [22].

Another approach to sparse array design and sensor selection is directly optimizing a performance metric. For example, [23] optimizes the confidence of linear parameter estimation. The Weiss-Weinstein bound for single-target DoA estimation has also been used to find sparse linear arrays, specifically in [24]. The method by which the arrays are found is a randomized search method, and only relatively small linear arrays are shown. In [25], a genetic algorithm is

used to optimize (among other metrics) the stochastic CRB, to design sparse linear arrays. The single-target CRB is used in [26] to analyze and design V-shape planar arrays. While most of the work mentioned so far considers far-field DoA estimation, the CRB for near-field localization has also been used to design arrays, such as the centro-symmetric linear arrays of [27]. Most of the previously mentioned optimized arrays used a search or other global optimization method. On the other hand, the CRB also has successfully been used in convex semidefinite programs (SDPs) [28], [29], [30], which allows for convergence and optimality guarantees [31].

The CRB for the estimation of target parameters in radar scenarios is perhaps most famously described by [32], where in particular the CRB is derived for multi-target angle of arrival estimation when the target waveforms are unknown. The examples treated are limited to linear arrays though. In [33], the CRB is derived for the time delay, Doppler shift, and DoA of a single target in a 3-D radar scenario. The single-target CRB has been used to define so-called isotropic arrays, which have a CRB which is independent of the target arrival angle [34].

The single-target CRB using a known waveform was used in [28] to perform sensor selection on uniform linear candidate arrays. To account for multi-target performance, despite using the single-target CRB, a maximum peak sidelobe level (PSL) constraint was added. Alternatively, all possible parameter values of a fixed number of targets can be considered (by gridding), which is what [29] proposed. When the gridding of the target parameter values is dense, however, and/or when there are many targets, the semi-definite constraint that is employed grows larger, which is the primary contributor to the computational complexity of SDPs [31]. The work of [30] proposed to mitigate this issue by limiting the number of targets to two. As in [28], the CRB that was used in [30] was based on the assumption that the received waveforms are known though. In practice, at the very least, the complex scaling of the received waveform is unknown, which leads to the tighter CRB presented in [32], [33]. These tighter bounds were used in [35], [36] in combination with the worst-case two-target concept from [30] to obtain sensor selections from a uniform linear and uniform planar candidate array, respectively, but they lacked generalization to arbitrary candidate array dimensions.

B. NOTATION, CONTRIBUTIONS & OUTLINE

Upright characters represent well-known constants such as $\mathrm{j} = \sqrt{-1}$, and operators such as $(\cdot)^{\mathsf{T}}$ and $(\cdot)^{\mathsf{H}}$, which are the complex conjugation, transpose and conjugate transpose operators, respectively. The Hadamard product, Kronecker product, and face-splitting (row-wise Kronecker) product are written as $\circ$, $\otimes$, and $\bullet$, respectively. Bold capital characters ($\boldsymbol{A}$) and bold lowercase characters ($\boldsymbol{a}$) represent matrices and vectors, respectively, while other italic characters, such as a, represent scalars. Calligraphic letters ($\mathcal{A}$) represent sets and distributions. An exception to this is that some special sets, such as the set of real numbers $\mathbb{R}$ and complex numbers $\mathbb{C}$, are written in 'blackboard bold'. We define $\mathcal{B} = \{0, 1\}$ and $\tilde{\mathcal{B}} = [0, 1]$. The function $\exp[\cdot]$ is element-wise exponentiation, $\mathrm{diag}(\boldsymbol{a})$ produces a diagonal matrix with $\boldsymbol{a}$ on its diagonal, and $\mathrm{vec}(\boldsymbol{A})$ produces a vector consisting of the concatenated columns of $\boldsymbol{A}$.

The contributions of this work can be summarized as

- Derivation of the CRB for DoA estimation of multiple deterministic unknown target waveforms using a 3-D array, highlighting the specific block structure that occurs in the Cramér-Rao Bound matrix (CRBM) for the 2-D and 3-D case. We assume the DoA and target waveforms to be deterministic, like [32], [33], in contrast to works such as [37] where those are assumed stochastic.
- Discussion of the properties of the two-target CRB and how the worst-case two-target CRB can relate to the PSL, a popular metric to control multi-target performance.
- Presentation of two SDP methods that can be used to obtain sensor selections on 3-D candidate arrays for the known DoA CRB and worst-case two-target CRB.

It may seem like we are focussing on a method for offline sensor selection, since our work focuses mostly on optimizing a metric that minimally depends on the scenario, e.g., the worst-case two-target CRB. Nevertheless, due to reasons mentioned before, such as the case of sensor outage, it may still be desirable to use the proposed sensor selection method in an online setting. Therefore, we present a convex SDP and discuss ways to make its optimization less intensive, such that the optimization may be completed within a reasonable time.

We describe the signal model and problem statement in Section II. In Section III, we derive the CRB for estimating the DoAs of multiple targets using a 3-D array, assuming unknown target waveforms. Using the CRB from Section III, we present a method of array element selection for DoA estimation in an unknown multi-target scenario. We evaluate the method using simulations in Section V and close with a discussion and conclusions in Section VI.

II. SIGNAL MODEL, ASSUMPTIONS & PROBLEM FORMULATION

We consider a receiver array of N identical, isotropic, and perfectly isolated receiving elements. Each receiving element is positioned at a unique location $\boldsymbol{x}_n \in \mathbb{R}^3$, where n is the index of a particular receive element. All N locations are collected in a matrix

$$\boldsymbol{X} = [\boldsymbol{x}_1 \quad \boldsymbol{x}_2 \quad \cdots \quad \boldsymbol{x}_N] \in \mathbb{R}^{3\times N}. \tag{1}$$

Under the narrowband and far-field assumptions, the DoA for the entire array can be well approximated by a single direction vector, so we can write the baseband received data matrix of the array, given K target signals and T temporal samples, as

$$\boldsymbol{Y} = \sum_{k=1}^{K} \boldsymbol{a}_k \boldsymbol{s}_k^{\mathsf{T}} + \boldsymbol{E} = \boldsymbol{A}\boldsymbol{S}^{\mathsf{T}} + \boldsymbol{E} \in \mathbb{C}^{N\times T}.$$

Here, the target waveform matrix is defined as

$$\boldsymbol{S} = [\boldsymbol{s}_1 \quad \cdots \quad \boldsymbol{s}_K] \in \mathbb{C}^{T\times K},$$

with $\mathbf{s}_k$ the temporal waveform related to the kth target. Further, the array response vectors and matrix are respectively given by

$$\boldsymbol{a}_k = \exp[\mathrm{j}\boldsymbol{X}^\mathsf{T}\boldsymbol{\omega}_k], \quad \boldsymbol{A} = \exp[\mathrm{j}\boldsymbol{X}^\mathsf{T}\boldsymbol{\Omega}] \in \mathbb{C}^{N\times K}, \tag{2}$$

where $\boldsymbol{\Omega}$ collects the target DoA vectors $\boldsymbol{\omega}_k$ such that

$$\boldsymbol{\Omega} = [\boldsymbol{\omega}_1 \quad \boldsymbol{\omega}_2 \quad \cdots \quad \boldsymbol{\omega}_K] \in \mathbb{R}^{3\times K}.$$

Please note that although we refer to the vectors $\boldsymbol{\omega}_k$ as directions, they only describe the directions of the targets but do not represent the physical angles directly. To convert between the $\boldsymbol{\omega}_k$ vectors and the azimuth and elevation angles, the carrier wavelength λ is needed:

$$\boldsymbol{\omega}_k = \frac{2\pi}{\lambda}[\cos\theta_k\cos\phi_k \quad \sin\theta_k\cos\phi_k\sin\phi_k]^\mathsf{T},$$

where θ_k and ϕ_k are the azimuth and elevation angles of the kth target, respectively.

Finally, the noise matrix $\boldsymbol{E}$ is assumed to be circularly-symmetric complex normal distributed and spatially and temporally uncorrelated with variance σ_e^2, i.e., $\boldsymbol{e} = \mathrm{vec}(\boldsymbol{E}) \sim \mathcal{CN}(\boldsymbol{0}, \sigma_e^2\boldsymbol{I})$. As a result, we have

$$\boldsymbol{y} = \mathrm{vec}\,(\boldsymbol{Y}) \sim \mathcal{CN}(\mathrm{vec}(\boldsymbol{A}\boldsymbol{S}^\mathsf{T})), \sigma_e^2\boldsymbol{I}. \tag{3}$$

For later use, it will also be of interest to introduce the vectorized versions of $\boldsymbol{S}$ and $\boldsymbol{\Omega}$, i.e., $\boldsymbol{s} = \mathrm{vec}(\boldsymbol{S})$, $\boldsymbol{\omega} = \mathrm{vec}(\boldsymbol{\Omega})$. Furthermore, the derivative of the array response vectors to the directions will be required:

$$\boldsymbol{D}_k = \frac{\partial \boldsymbol{a}_k}{\partial \boldsymbol{\omega}_k} = \mathrm{j}\boldsymbol{X}^\mathsf{T} \bullet \exp[\mathrm{j}\boldsymbol{X}^\mathsf{T}\boldsymbol{\omega}_k] \in \mathbb{C}^{N\times 3},$$

$$\boldsymbol{D} = [\boldsymbol{D}_1 \quad \boldsymbol{D}_2 \quad \cdots \quad \boldsymbol{D}_K] \in \mathbb{C}^{N\times 3K}. \tag{4}$$

A. PROBLEM FORMULATION

Consider a length-N binary vector $\boldsymbol{p} \in \mathcal{B}^N$. We will use this vector $\boldsymbol{p}$ to indicate which of the elements of the full candidate array we want to use. When p_n, the nth element of $\boldsymbol{p}$, equals one, we select the nth element of the candidate array. If it is zero, we do not. We consider in this work the case where we want to select a fixed number of sensors, M. Thus, $\boldsymbol{p}$ should contain exactly M ones.

To generate our new array response vectors, we use $\boldsymbol{p}$ to construct a selection matrix $\boldsymbol{\Phi} \in \mathcal{B}^{M\times N}$. The matrix $\boldsymbol{\Phi}$ is equal to the matrix $\mathrm{diag}(\boldsymbol{p})$ with the all-zero rows removed. As an example, consider

$$\boldsymbol{p} = [1 \quad 0 \quad 1]^\mathsf{T} \quad \Leftrightarrow \quad \boldsymbol{\Phi} = \begin{bmatrix} 1 & 0 & 0 \\ 0 & 0 & 1 \end{bmatrix}.$$

The matrix $\boldsymbol{\Phi}$ has some useful properties that we will need in the following sections, namely

$$\boldsymbol{\Phi}\boldsymbol{\Phi}^\mathsf{T} = \boldsymbol{I}, \qquad \boldsymbol{\Phi}^\mathsf{T}\boldsymbol{\Phi} = \mathrm{diag}(\boldsymbol{P}) = \boldsymbol{P}, \qquad \boldsymbol{P}^2 = \boldsymbol{P}. \tag{5}$$

To obtain the array response vectors and their derivative to the related direction after sensor selection, we simply apply $\boldsymbol{\Phi}$:

$$\boldsymbol{A} \to \boldsymbol{\Phi}\boldsymbol{A} \in \mathbb{C}^{M\times K}, \qquad \boldsymbol{D} \to \boldsymbol{\Phi}\boldsymbol{D} \in \mathbb{C}^{M\times 3K}. \tag{6}$$

The problem of sensor selection is then to find a vector $\boldsymbol{p}^\star$ which performs no worse in a chosen metric than any other vector $\boldsymbol{p}$ of the same length and with the same number of non-zero elements, i.e.,

$$\underset{\boldsymbol{p}\in\mathcal{B}^N}{\text{minimize}}\ f(\boldsymbol{p}) \quad \text{subject to} \quad \boldsymbol{1}^\mathsf{T}\boldsymbol{p} = M. \tag{7}$$

We elaborate and motivate our choice of $f(\boldsymbol{p})$ in Sections III and IV-B.

III. THE MULTI-TARGET CRAMÉR-RAO BOUND FOR 3-D ARRAYS

To perform sensor selection, we need a metric to evaluate and compare different sets of sensors. We would prefer a method that is agnostic to the DoA estimator, in particular for offline selection. If we manage that, then a deployed system does not need hardware adjustments due to an estimator update. Of course, using a sensor selection method that is specifically optimized for a specific estimator should perform the best for that estimator. However, by using the CRB as we propose, the resulting sensor selections will also be close to optimal for an efficient estimator.

From previous work, it is known that the CRBs for the waveforms, DoA, range and velocity are not affected by the noise variance being known or unknown [32], [33]. Therefore, we consider the unknown parameter vector

$$\boldsymbol{\eta} = \begin{bmatrix} \mathrm{Re}\begin{bmatrix}\boldsymbol{s}^\mathsf{T}\end{bmatrix} & \mathrm{Im}\begin{bmatrix}\boldsymbol{s}^\mathsf{T}\end{bmatrix} & \boldsymbol{\omega}^\mathsf{T}\end{bmatrix}^\mathsf{T}.$$

Theorem 1: The CRB for DoA estimation from the data distribution in (3) is given by

$$\mathrm{CRB}_{\boldsymbol{\omega}\boldsymbol{\omega}}(\boldsymbol{\Omega}) = \left(\frac{2T}{\sigma_e^2}\mathrm{Re}\left[\boldsymbol{D}^\mathsf{H}(\boldsymbol{I} - \boldsymbol{A}(\boldsymbol{A}^\mathsf{H}\boldsymbol{A})^{-1}\boldsymbol{A}^\mathsf{H})\boldsymbol{D}\circ\tilde{\boldsymbol{R}}^\mathsf{T}\right]\right)^{-1}, \tag{8}$$

where $\tilde{\boldsymbol{R}} = \boldsymbol{R}\otimes\boldsymbol{J}_3 \in \mathbb{C}^{3K\times 3K}$, $\boldsymbol{R}^\mathsf{T} = \frac{1}{T}\boldsymbol{S}^\mathsf{H}\boldsymbol{S}$, and $\boldsymbol{J}_D$ is a $D\times D$ matrix of ones.

Proof: See Appendix A. ■

To make (8) a selection-dependent metric, we simply replace all occurrences of $\boldsymbol{A}$ and $\boldsymbol{D}$ by $\boldsymbol{\Phi}\boldsymbol{A}$ and $\boldsymbol{\Phi}\boldsymbol{D}$, respectively, as per (6). Applying this substitution and the properties of the $\boldsymbol{\Phi}$ matrix in (5) to the CRB in (8) leads to a selection-dependent equivalent Fisher information matrix (EFIM):

$$\mathrm{CRB}^{-1}_{\boldsymbol{\omega}\boldsymbol{\omega}}(\boldsymbol{\Omega}, \boldsymbol{p}) = \frac{2T}{\sigma_e^2}\mathrm{Re}\left[\boldsymbol{D}^\mathsf{H}\boldsymbol{P}(\boldsymbol{I} - \boldsymbol{A}(\boldsymbol{A}^\mathsf{H}\boldsymbol{P}\boldsymbol{A})^{-1}\boldsymbol{A}^\mathsf{H})\boldsymbol{P}\boldsymbol{D}\circ\tilde{\boldsymbol{R}}^\mathsf{T}\right]. \tag{9}$$

An EFIM is simply the inverse of a chosen block of the CRB matrix.

When considering planar and linear arrays, we do not need to consider the full $3K$-by-$3K$ CRB in (9). When the array

exists in a plane (line), we can find an orientation and reference for the sensor position matrix $\boldsymbol{X}$ in (1), which leads to the last row (last two rows) of $\boldsymbol{X}$ containing only zeros. This means that we can truncate the CRB by removing every third column and row for the planar case, and every second and third column and row for the linear case. Initial results from using the multi-target selection-dependent CRB for sensor selection in the linear and planar case have been published in [35] and [36], respectively.

While we chose to take the derivative towards $\boldsymbol{\omega}_k$ in (4), we can also take the derivative towards $\boldsymbol{\theta}_k = [\theta_k \quad \phi_k]^\mathsf{T}$:

$$\boldsymbol{D}_{\boldsymbol{\theta}_k} = \frac{\partial \boldsymbol{a}_k}{\partial \boldsymbol{\theta}_k} = \mathrm{j}\boldsymbol{X}^\mathsf{T} \frac{\partial \boldsymbol{\omega}_k}{\partial \boldsymbol{\theta}_k} \bullet \exp[\mathrm{j}\boldsymbol{X}^\mathsf{T}\boldsymbol{\omega}_k] \in \mathbb{C}^{N\times 2}\,,$$

$$\frac{\partial \boldsymbol{\omega}_k}{\partial \boldsymbol{\theta}_k} = \frac{2\pi}{\lambda}\begin{bmatrix} -\sin\theta_k\cos\phi_k & -\cos\theta_k\sin\phi_k \\ \cos\theta_k\cos\phi_k & -\sin\theta_k\sin\phi_k \\ 0 & \cos\phi_k \end{bmatrix}.$$

Replacing the $\boldsymbol{D}$ matrices in (9) by using the partial derivatives $\boldsymbol{D}_{\boldsymbol{\theta}_k}$ instead, we can obtain a CRB that depends directly on the physical angles. However, for this work we mainly use $\mathrm{CRB}_{\boldsymbol{\omega}\boldsymbol{\omega}}(\boldsymbol{\Omega}, \boldsymbol{p})$, since it has some attractive properties that we will discuss and exploit in Section IV-B and IV-C. We make an exception in Section IV-A, where we briefly discuss the use of $\boldsymbol{D}_{\boldsymbol{\theta}_k}$.

IV. ARRAY ELEMENT SELECTION METHOD

While we have introduced a metric that will be useful in determining the performance of sparse arrays, we need a scalar cost function for (7). There are numerous ways to obtain cost functions from matrix metrics. In particular, E-optimality (minimizing the largest eigenvalue), D-optimality (minimizing the log of the determinant) and A-optimality (minimizing the trace) appear throughout literature as popular choices, each with their own advantages and disadvantages [38], [39]. In addition to a scalarization, there are some other difficulties with the CRB as well: The size of the CRB depends on the number of targets, and the CRB depends on the DoAs of those targets, both of which are typically unknown. The way we propose to tackle these difficulties is by considering a specific case, the worst-case two-target CRB, but first, we will consider another simplification: assuming that the DoAs are known.

A. ASSUMING THE DOAS KNOWN

We can mitigate many of the previously mentioned challenges by assuming the target DoAs are known. This assumption is not so applicable to surveillance radar applications, but in tracking radar and when using radar to inspect known infrastructure, it is typical to have an estimate of the target DoAs already. Before we continue deriving our cost function, we first make the following assumption.

Assumption 1: The signals reflected by the targets are orthogonal, i.e.,

$$\boldsymbol{R} = \mathrm{diag}(\boldsymbol{r})\,,$$

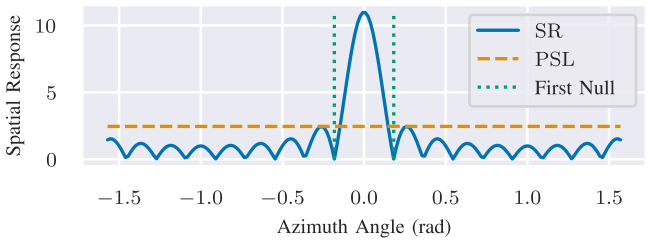

FIGURE 1. Example spatial response for a ULA of 11 elements using a matched filter aimed at 0 rad (broadside).

where $\boldsymbol{r} \in \mathbb{R}^K$ is a vector containing the target signal powers.

Assumption 1 is a fair assumption when T is large and the signals are affected uniquely by, for example, radar cross-section (RCS) fluctuations and Doppler shifts. Another scenario where the received signals can be orthogonal is when targets emit their own signals. In this case, we find the EFIM for the physical angles $\boldsymbol{\theta}_k$ of the kth target, neglecting constant factors,[1] to be

$$\boldsymbol{F}_k(\boldsymbol{\Theta}, \boldsymbol{P}) = \mathrm{Re}\left[\boldsymbol{D}_{\boldsymbol{\theta}_k}^\mathsf{H}\boldsymbol{P}(\boldsymbol{I} - \boldsymbol{A}(\boldsymbol{A}^\mathsf{H}\boldsymbol{P}\boldsymbol{A})^{-1}\boldsymbol{A}^\mathsf{H})\boldsymbol{P}\boldsymbol{D}_{\boldsymbol{\theta}_k}\right],$$

where $\boldsymbol{\Theta} = [\boldsymbol{\theta}_1 \quad \cdots \quad \boldsymbol{\theta}_K]$.

With this EFIM, we can formulate the following worst-case sensor selection problem

$$\begin{aligned} \min_{\boldsymbol{p}\in\mathcal{B}^N} \max_k \quad & \mathrm{tr}(\boldsymbol{F}_k^{-1}(\boldsymbol{\Theta}, \boldsymbol{p})) \\ \text{subject to} \quad & \mathbf{1}^\mathsf{T}\boldsymbol{p} = M\,. \end{aligned} \tag{10}$$

To scalarize the cost, we use the trace function (A-optimality) since it optimizes the mean of the estimation performance of the three coordinates of the DoA.

But what if we want an array that works for unknown targets? For that we advocate using the worst-case two-target CRB, where the two targets can be anywhere.

B. PROPOSED METRIC: THE WORST-CASE TWO-TARGET CRAMÉR-RAO BOUND

Mitigating unknown interference and clutter is a common problem in radar signal processing. As discussed in Section I, popular metrics to quantify the mitigation are usually related to sidelobe levels of the array response, such as the PSL. The sidelobe levels depend on the receiver that is used, such as the matched filter, which might be the most common receiver. For example, when a matched filter is used and steered at $\boldsymbol{\omega}_1$, the spatial response at $\boldsymbol{\omega}_2$ is given by

$$\mathrm{SR}(\boldsymbol{\omega}_1, \boldsymbol{\omega}_2) = |\boldsymbol{a}^\mathsf{H}(\boldsymbol{\omega}_1)\boldsymbol{a}(\boldsymbol{\omega}_2)|\,. \tag{11}$$

An example of such a spatial response for a ULA and $\omega_1 = 0$ is given in Fig. 1. Here, the first nulls are also indicated, which together specify the mainlobe width or first null beamwidth

[1] Constant factors will only scale the optimal value, not the optimal arguments, so they can be omitted.

(FNBW). Note that the mainlobe width may change based on $\boldsymbol{\omega}_1$.

To obtain measures such as the PSL, the spatial response needs to be evaluated for all values of $\boldsymbol{\omega}_1$ and $\boldsymbol{\omega}_2$, as in

$$\begin{aligned} \text{PSL} = \max_{\boldsymbol{\omega}_1,\boldsymbol{\omega}_2} \quad & \text{SR}(\boldsymbol{\omega}_1,\boldsymbol{\omega}_2)\,, \\ \text{s.t.} \quad & \|\boldsymbol{\omega}_2-\boldsymbol{\omega}_1\| \geq \alpha(\boldsymbol{\omega}_1)\,, \end{aligned}$$

where $\alpha(\boldsymbol{\omega}_1)$ is used to make sure the mainlobe is excluded from the evaluation. When the array response vectors are given by (2), the spatial response only depends on the difference

$$\Delta\boldsymbol{\omega} = \boldsymbol{\omega}_2 - \boldsymbol{\omega}_1\,,$$

and (11) simplifies to

$$\text{SR}(\Delta\boldsymbol{\omega}) = |\boldsymbol{a}^{\mathsf{H}}(0)\boldsymbol{a}(\Delta\boldsymbol{\omega})|\,.$$

Finding the PSL then also simplifies to

$$\begin{aligned} \text{PSL} = \max_{\Delta\boldsymbol{\omega}} \quad & \text{SR}(\Delta\boldsymbol{\omega})\,, \\ \text{s.t.} \quad & \|\Delta\boldsymbol{\omega}\| \geq \alpha\,. \end{aligned}$$

The PSL is used as a metric for unknown multi-target performance because it describes the worst-case interference that one target can inflict upon another. However, it relies on the receiver that is used, and for different receivers the expression for the spatial response may be more complex than (11). So, in the spirit of the PSL, we would like to use a worst-case two-target metric, but one that does not depend on the receiver, i.e., the CRB. Since the CRB can be used to describe performance independent of the receiver, it can also be used to evaluate array performance when receivers that have super-resolution capabilities are used.

Proposition 1: Given Assumption 1, the two-target CRB only depends on the DoA difference of the targets, $\Delta\boldsymbol{\omega}$, not their absolute DoAs, the CRBs of the two targets are equal up to a scaling of their powers, and

$$\text{CRB}_{\boldsymbol{\omega}\boldsymbol{\omega}}(\Delta\boldsymbol{\omega},\boldsymbol{p}) = \text{CRB}_{\boldsymbol{\omega}\boldsymbol{\omega}}(-\Delta\boldsymbol{\omega},\boldsymbol{p})\,. \tag{12}$$

Proof: See Appendix B. ■

Let $\boldsymbol{F}(\Delta\boldsymbol{\omega},\boldsymbol{p})$ be the EFIM for the DoA of a target, neglecting constant factors:

$$\boldsymbol{F}(\Delta\boldsymbol{\omega},\boldsymbol{p}) = \ddot{\boldsymbol{Z}}(\boldsymbol{p}) - \dot{\boldsymbol{Z}}^{\mathsf{H}}(\Delta\boldsymbol{\omega},\boldsymbol{p})\boldsymbol{Z}^{-1}(\Delta\boldsymbol{\omega},\boldsymbol{p})\dot{\boldsymbol{Z}}(\Delta\boldsymbol{\omega},\boldsymbol{p})\,,$$

where $\boldsymbol{Z}(\Delta\boldsymbol{\omega},\boldsymbol{p})$, $\dot{\boldsymbol{Z}}(\Delta\boldsymbol{\omega},\boldsymbol{p})$ and $\ddot{\boldsymbol{Z}}(\boldsymbol{p})$ are given by (22) to (24) in Appendix B, and are linear in $\boldsymbol{p}$.

Using $\boldsymbol{F}(\Delta\boldsymbol{\omega},\boldsymbol{p})$, we formulate our sensor selection optimization problem as

$$\begin{aligned} \underset{\boldsymbol{p}\in\mathcal{B}^N}{\text{minimize}} \quad & \underset{\Delta\boldsymbol{\omega}\in\mathcal{D}_+}{\text{maximize}} \quad \text{tr}(\boldsymbol{F}^{-1}(\Delta\boldsymbol{\omega},\boldsymbol{p})) \\ \text{subject to} \quad & \mathbf{1}^{\mathsf{T}}\boldsymbol{p} = M\,, \end{aligned} \tag{13}$$

where $\mathcal{D}_+$ is the set of direction differences to be considered in the worst-case evaluation. The set $\mathcal{D}_+$ can be made smaller such that it contains no equivalent direction differences (see (12)), which helps to lower the complexity of the optimization problem. Furthermore, if the direction difference becomes too small, $\boldsymbol{F}(\Delta\boldsymbol{\omega},\boldsymbol{p})$ will become ill-conditioned, so a minimum direction difference should be enforced in choosing $\mathcal{D}_+$. Due to Proposition 1, optimization for only $\boldsymbol{F}(\Delta\boldsymbol{\omega},\boldsymbol{p})$ is also sufficient in optimizing the worst case, since the EFIMs of the targets are equal up to a scaling given by their power ratio. To scalarize the cost, we used the trace function (A-optimality) since it optimizes the mean of the estimation performance of the three coordinates of the DoA.

Since it is not immediately obvious how to optimize the problem in (13), we show a convex relaxation of the problem in Section IV-C.

C. RELAXATIONS FOR EFFICIENT OPTIMIZATION

Our first step in relaxing the problem in (13) is eliminating the maximization over $\Delta\boldsymbol{\omega}$ by discretizing the direction difference set $\mathcal{D}_+$. Additionally, we relax the binary constraint on $\boldsymbol{p}$ to a box constraint on an intermediate variable $\tilde{\boldsymbol{p}}$. By doing that, we can reformulate the minimax problem as

$$\begin{aligned} \underset{\tilde{\boldsymbol{p}}\in\tilde{\mathcal{B}}^N,\boldsymbol{C}}{\text{minimize}} \quad & \text{tr}(\boldsymbol{C}) \\ \text{subject to} \quad & \mathbf{1}^{\mathsf{T}}\tilde{\boldsymbol{p}} = M \\ & \boldsymbol{F}(\Delta\boldsymbol{\omega},\tilde{\boldsymbol{p}}) \succeq \boldsymbol{C}^{-1}\,,\ \forall\Delta\boldsymbol{\omega}\in\mathcal{D}_+\,. \end{aligned} \tag{14}$$

Then, using repeated application of the Schur complement [38, A.5.5] (see Appendix C) we may obtain the following convex SDP:

$$\begin{aligned} \min_{\tilde{\boldsymbol{p}}\in\tilde{\mathcal{B}}^N,\boldsymbol{C},\boldsymbol{G}} \quad & \text{tr}(\boldsymbol{C}) \\ \text{subject to} \quad & \mathbf{1}^{\mathsf{T}}\tilde{\boldsymbol{p}} = M\,, \quad \begin{bmatrix} \ddot{\boldsymbol{Z}}(\tilde{\boldsymbol{p}}) - \boldsymbol{G} & \boldsymbol{I} \\ \boldsymbol{I} & \boldsymbol{C} \end{bmatrix} \succeq \mathbf{0} \\ & \begin{bmatrix} \boldsymbol{G} & \dot{\boldsymbol{Z}}^{\mathsf{H}}(\Delta\boldsymbol{\omega},\tilde{\boldsymbol{p}}) \\ \dot{\boldsymbol{Z}}(\Delta\boldsymbol{\omega},\tilde{\boldsymbol{p}}) & \boldsymbol{Z}(\Delta\boldsymbol{\omega},\tilde{\boldsymbol{p}}) \end{bmatrix} \succeq \mathbf{0}\,,\ \forall\Delta\boldsymbol{\omega}\in\mathcal{D}_+\,, \end{aligned} \tag{15}$$

where all the matrix inequalities are linear in the optimization variables. Similarly, we can relax (10) to

$$\begin{aligned} \min_{\tilde{\boldsymbol{p}}\in\tilde{\mathcal{B}}^N,\boldsymbol{C},\boldsymbol{G}} \quad & \text{tr}(\boldsymbol{C}) \\ \text{subject to} \quad & \mathbf{1}^{\mathsf{T}}\tilde{\boldsymbol{p}} = M\,, \quad \begin{bmatrix} \ddot{\boldsymbol{Z}}(\tilde{\boldsymbol{p}}) - \boldsymbol{G} & \boldsymbol{I} \\ \boldsymbol{I} & \boldsymbol{C} \end{bmatrix} \succeq \mathbf{0}\,, \\ & \begin{bmatrix} \boldsymbol{G} & \boldsymbol{D}_{\theta_k}^{\mathsf{H}}\tilde{\boldsymbol{P}}\boldsymbol{A} \\ \boldsymbol{A}^{\mathsf{H}}\tilde{\boldsymbol{P}}\boldsymbol{D}_{\theta_k} & \boldsymbol{A}^{\mathsf{H}}\tilde{\boldsymbol{P}}\boldsymbol{A} \end{bmatrix} \succeq \mathbf{0}\,,\ \forall k = 1,\ldots,K\,, \end{aligned} \tag{16}$$

where $\tilde{\boldsymbol{p}} = \text{diag}(\tilde{\boldsymbol{p}})$.

To estimate the optimal selection vector $\boldsymbol{p}$ from the continuous vector $\tilde{\boldsymbol{p}}$ obtained from solving (15), we use a randomized rounding procedure [29].

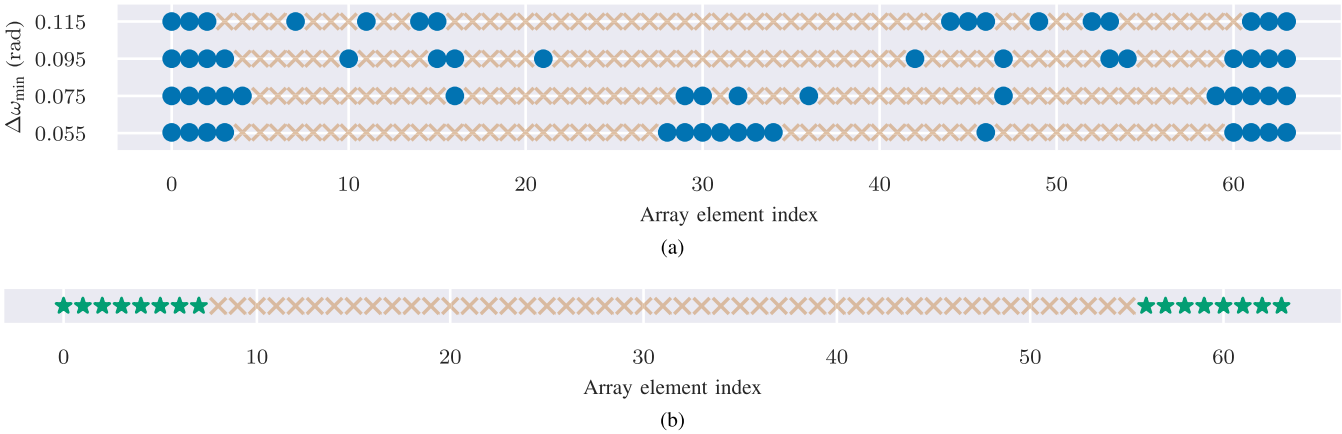

FIGURE 2. Example of sparse array results using a ULA candidate array for $(N, M) = (128, 32)$ with (a) our proposed method and (b) using (17). The $\Delta\omega_{\min}$ is varied to construct different sets $\mathcal{D}_+$.

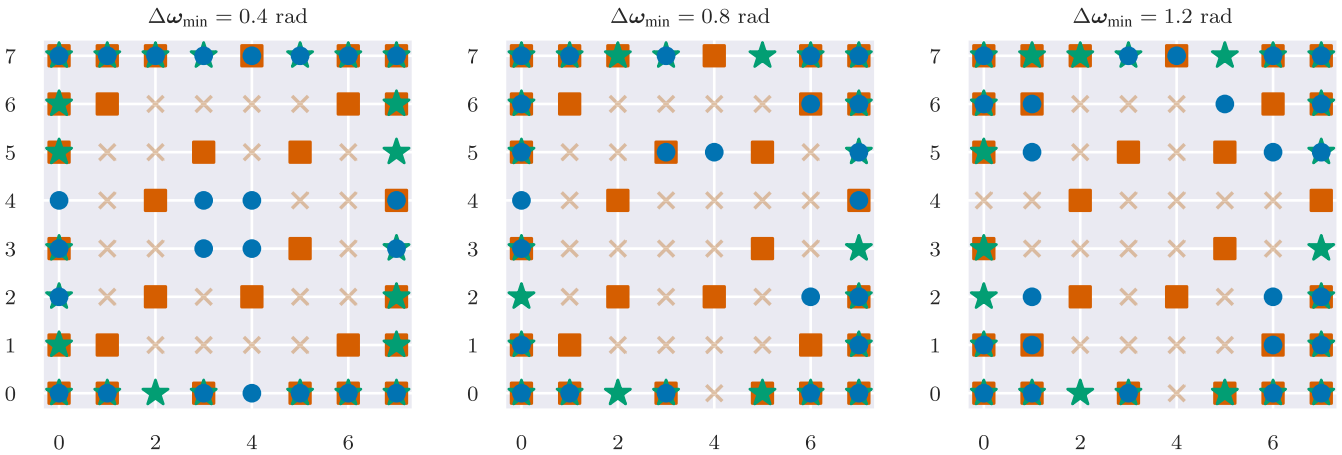

FIGURE 3. Example sparse array results for $(N, M) = (8 \times 8, 24)$. Blue dots indicate elements selected by our method, while green stars are those selected by (17). The squares are the CRA, and the crosses are those positions that are not selected by any of the methods.

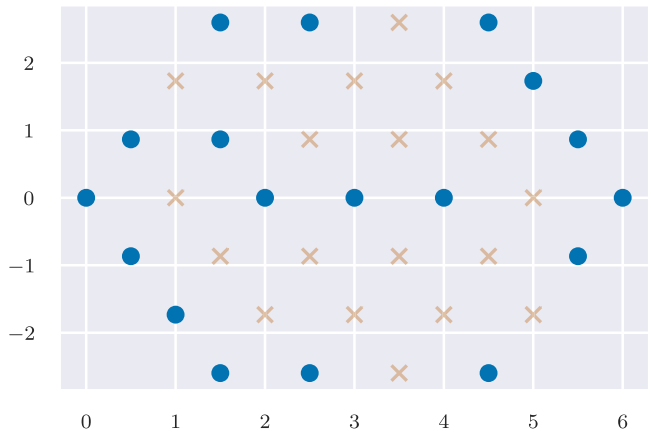

FIGURE 4. Example sparse array result for a honeycomb candidate array.

Since the problem (15) is a convex SDP, we could solve it using off-the-shelf solvers such as the free open-source software projects CVXPY [40] and CVXOPT [41]. However, SDPs scale primarily in the number and size of the semidefinite constraints [31], so the process of solving the problems using SDP solvers may still be computationally complex if $\mathcal{D}_+$ is large and/or densely sampled. To mitigate this, a user may want to evaluate a size of $\mathcal{D}_+$ that gives acceptable performance in terms of complexity and quality, and/or reduce the size of the individual linear matrix inequalitys (LMIs) if the candidate array is linear or planar as in [35] and [36], respectively.

V. NUMERICAL STUDY OF PERFORMANCE

To show the effectiveness of our proposed methods, we present in this section a number of simulation results. We will present some examples of sparse arrays that result from our methods, show some example beampatterns with the associated integrated sidelobe levels (ISLs) and PSLs that appear when using these arrays, and we will show the CRB results

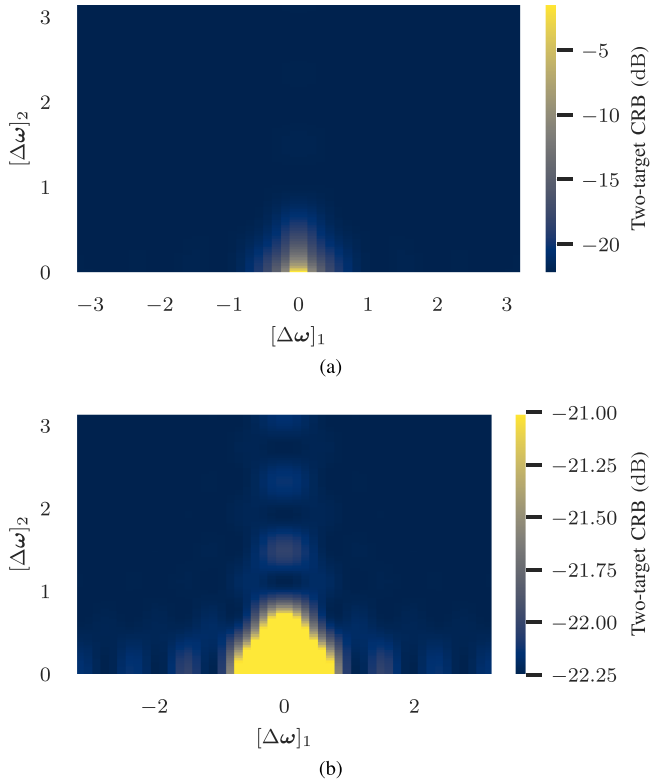

FIGURE 5. Two-target CRB dependence on $\Delta\omega$ for a full eight-by-eight UPA. While (a) shows the full range of values, (b) labels all values greater than or equal to -21 dB equally.

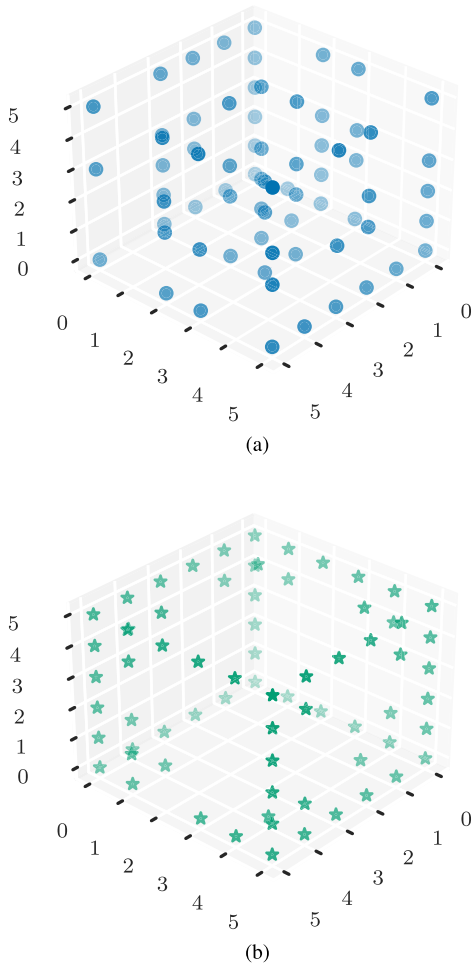

FIGURE 6. Example sparse array results for $(N, M) = (6 \times 6 \times 6, 72)$ with (a) our method and (b) using (17). The hues indicate depth.

from Monte Carlo simulations. Our methods are compared to some other methods as discussed in Section V-A.

Unless specified otherwise, we have used 100 Monte Carlo trials, 100 randomized rounding attempts, and uniform half-wavelength spacing in the candidate arrays.

A. BENCHMARKS

Here we briefly introduce some existing methods that we will compare our method against. The first is simply random selection, where we simply take an N-length vector of zeros and place M ones at random indices of the vector, as the resulting selection vector.

Second, we consider single-target optimization, where we set $K = 1$ and solve (13). For $K = 1$ the problem reduces to

$$\begin{aligned} \underset{\tilde{\boldsymbol{p}}\in\tilde{\mathcal{B}}^N,\boldsymbol{C},\boldsymbol{G}}{\text{minimize}} \quad & \operatorname{tr}(\boldsymbol{C}) \\ \text{subject to} \quad & \mathbf{1}^{\mathsf{T}}\tilde{\boldsymbol{p}} = M \\ & \begin{bmatrix} \ddot{\boldsymbol{Z}}(\tilde{\boldsymbol{p}}) - \boldsymbol{G} & \boldsymbol{I} \\ \boldsymbol{I} & \boldsymbol{C} \end{bmatrix} \succeq \mathbf{0}, \quad \begin{bmatrix} \boldsymbol{G} & \boldsymbol{X}\tilde{\boldsymbol{p}} \\ \tilde{\boldsymbol{p}}^{\mathsf{T}}\boldsymbol{X}^{\mathsf{T}} & M \end{bmatrix} \succeq \mathbf{0}. \end{aligned} \tag{17}$$

We see in our simulations that the solutions to (17) seem to select the sensors that are the furthest from the center of the candidate array, see Figs. 2(b), 3, and 6(b). Thus, explicitly performing the optimization may be unnecessary.

Third, we compare to the CRA introduced in [7]. In the case of a square candidate array with an odd number of rows and columns, the CRA results in the MRA. MRA is another popular sparse array concept, which minimizes the number of duplicate distances within the array, but it is difficult to find for large amounts of sensors. The CRA has a fixed sparsity M for a given rectangular candidate array, so when we compare the other methods to the CRA, we fix M to this value. When we show results for different values of M, we omit the CRA from the comparison.

Last, we compare to the BA [14], [15], [16]. This is only defined for planar candidate arrays with a clearly defined convex boundary. It simply selects all the elements that reside on the boundary of the candidate array. The sparsity M of this method is also fixed given a candidate array. In the case of a rectangular candidate array, the sparsity is exactly the same as for the CRA. As such, for the results we show for fixed M given the candidate array, we can make a fair comparison. For the results we show for different values of M, we exclude the BA from the comparison, just like we do with the CRA.

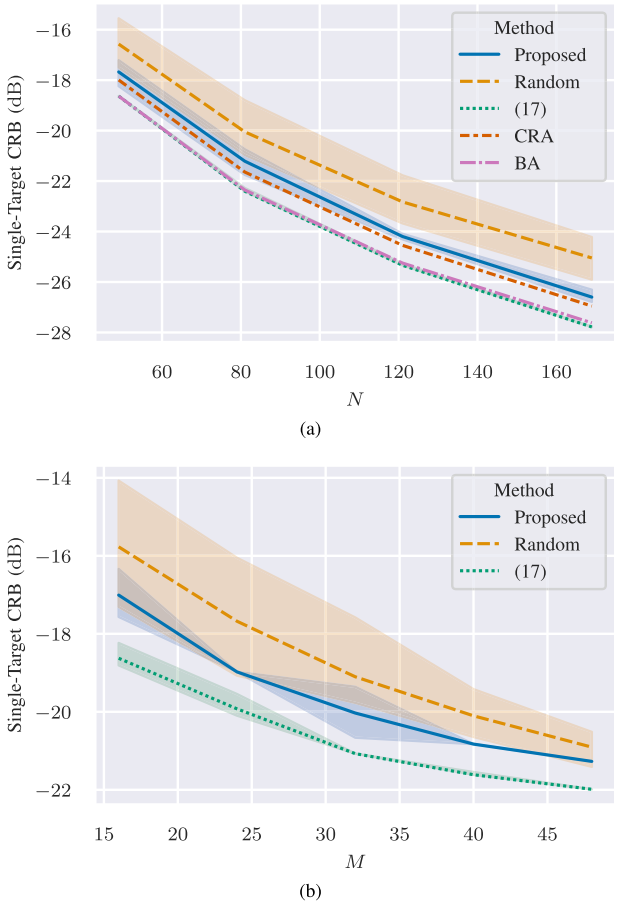

FIGURE 7. Single-target CRB performance for (a) varying square candidate array sizes and $M = N/4$, and (b) $N = 64$ and varying sparsities.

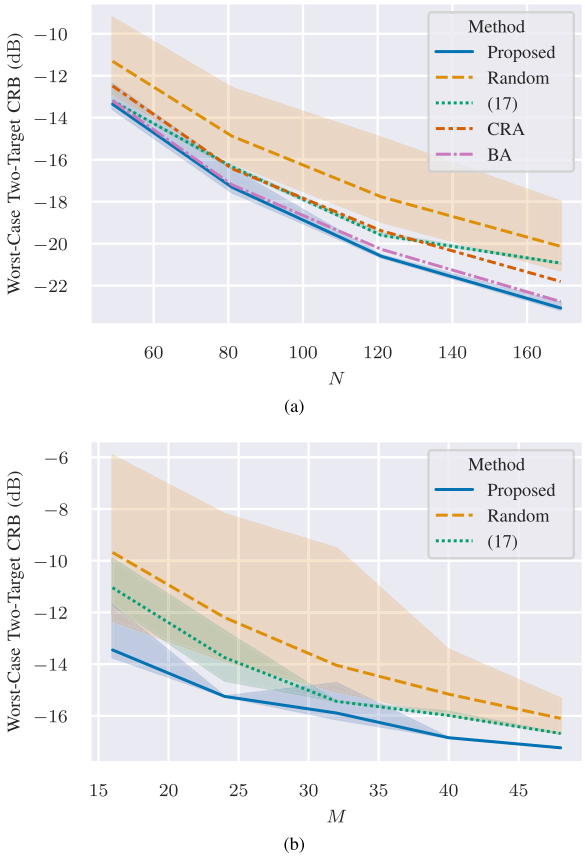

FIGURE 8. Worst-case two-target CRB performance for (a) varying square candidate array sizes and $M = N/4$, and (b) $N = 64$ and varying sparsities.

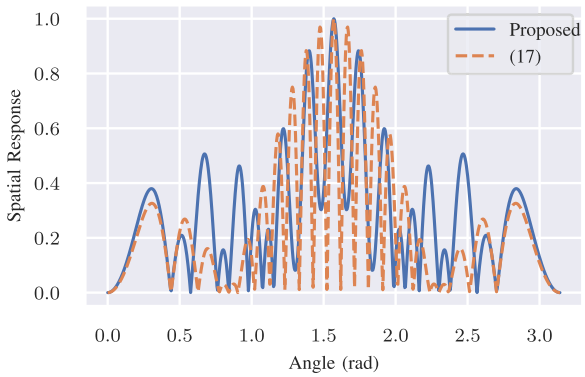

FIGURE 9. Spatial response of the sparse arrays in Fig. 2 and from (17). The mainlobe is aimed at $\theta = \frac{\pi}{2}$.

B. SIMULATION RESULTS

In Figs. 2, 3, 4, and 6, blue dots are used to indicate elements selected by the proposed method, while green stars are those selected by (17). Squares indicate the CRA, and the crosses are those candidate elements that are not selected by any of the methods present in that figure. In Figs. 7 and 8, the same colors are used to differentiate the methods.

In Figs. 2 and 3, we show some results of sparse arrays resulting from our method compared to the benchmarks. We varied the minimum direction difference in the construction of $\mathcal{D}_+$ to show it has a significant effect on the resulting arrays. For small minimum differences, the arrays resulting from our method have approximately half of the elements clustered in the center of the candidate array, with the rest of the elements as far as possible to the edges of the candidate array. Note that while some symmetry is expected in the resulting arrays, it is not always realized due to the specific values of N and M, and due to the randomized rounding procedure, since elements of equal weight in $\tilde{\boldsymbol{p}}$ may not all be selectable. To emphasize that our method does not require a uniform candidate array, we show the results based on a honeycomb candidate array in Fig. 4. Since its structure is trivial, the BA is omitted from the figures to reduce clutter.

As the minimum direction difference, $\Delta\omega_{\min}$, increases, the array elements that were in the center of the array before now move further and further out. We do not note a similar change when we keep $\Delta\omega_{\min}$ small and change the maximum direction difference in $\mathcal{D}_+$, so this may indicate that the minimum direction difference is the determining factor. To investigate this, we have plotted the two-target CRB values for different values of $\Delta\boldsymbol{\omega}$ in Fig. 5 when a full eight-by-eight UPA is used. We see that there is a region where the CRB

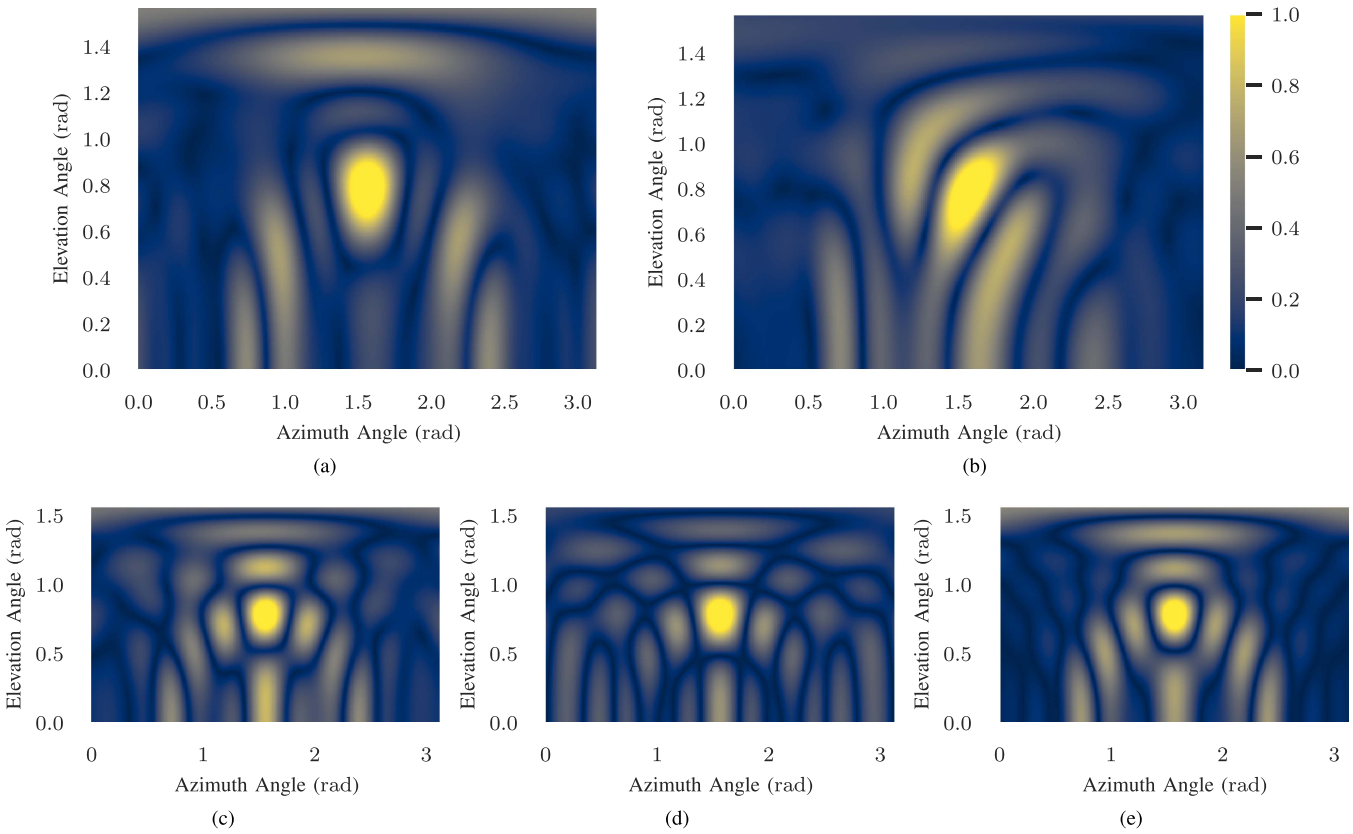

FIGURE 10. Spatial response of (a) the proposed method, (b) the known target optimization from (16) (with three targets at $\Theta = \begin{bmatrix} \frac{\pi}{2} & 1 & 2.2 \\ \frac{\pi}{4} & 0.5 & 0.5 \end{bmatrix}$), (c) the solution of (17), (d) the CRA, and (e) the BA. The mainlobe is aimed at $(\theta, \phi) = (\frac{\pi}{2}, \frac{\pi}{4})$ and $(N, M) = (9 \times 9, 32)$.

is non-increasing with increasing $\Delta\boldsymbol{\omega}$ and significantly larger than the CRB outside this region. If the desired $\Delta\boldsymbol{\omega}_{\min}$ is in this region, it may suffice to optimize (15) only for this $\Delta\boldsymbol{\omega}_{\min}$, instead of a set, yielding significantly reduced computational complexity. This is due to the fact that the primary contributor to computational complexity in solving SDPs is the size of the LMI constraint [31]. The size of this discussed region is difficult to predict unfortunately, since it depends on the specific sparse array. We have found empirically, however, that this monotonic region does not shrink in size compared to the full selection. It is however entirely possible that outside of this peak region, other peaks of comparable height are found when evaluating sparse arrays. Thus, the choice of optimizing over a large set $\mathcal{D}_+$ or a smaller set where all $|\Delta\boldsymbol{\omega}| = \Delta\omega_{\min}$ comes down to computational complexity versus worst-case robustness. To construct an example 3-D array, a smaller set $\mathcal{D}_+$ is used. We construct $\mathcal{D}_+$ by sampling 128 approximately equidistant points on a sphere of radius $\Delta\boldsymbol{\omega}_{\min} = 0.3$ using Fibonacci's method [42]. The result of the proposed method with this $\mathcal{D}_+$ using a uniform cube array as candidate is presented in Fig. 6.

Next, we look at the resulting single-target and worst-case two-target CRB results for the different methods. To generate the results, we have used a UPA candidate array and a $\Delta\boldsymbol{\omega}_{\min} = N/4$, which lies in the non-increasing region discussed previously. The single-target and two-target worst-case CRB results are given in Figs. 7 and 8, respectively. Since our method and some benchmarks include a randomized step, we have included in the figures the results of 100 random trials. The shaded regions in Figs. 7 and 8 indicate the minimum and maximum results of these 100 trials, while the lines indicate the mean. In practice, the best result out of some number of randomized rounding trials would be picked, so the shaded regions give some indication of the reliability of the randomized rounding. We note that the boundary array performs very close to optimal in both CRB metrics, but the boundary array is, of course, very limited in terms of the candidate arrays that can be used and the desired sparsity, M, that can be realized (which is fixed). Hence, its results, and those of the CRA for the same reason, have been omitted from Figs. 7(b) and 8(b).

When looking at some beampatterns produced by our method, compared to the known- and single-target CRB optimization, we find that our method naturally produces lower PSLs. In Fig. 9, we see an example of a beampattern steered to $\frac{\pi}{2}$ when using linear arrays. The result of Fig. 2 for $\Delta\boldsymbol{\omega}_{\min} = 0.055$ is used for our proposed method, and it is being compared to the result of (17). In Fig. 10, we see an example of the beampattern when the beamformer is steered to $\pi/2$ rad in azimuth and $\pi/4$ rad in elevation. We observe that the sidelobes

close to the mainlobe are significantly lower in magnitude with our sparse array in Figs. 9 and 10(a). This is, of course, at the cost of mainlobe width. In Fig. 10(b), the known target optimization result of (16) is shown with $\boldsymbol{\Theta} = \begin{bmatrix} \pi/2 & 1 & 2.2 \\ \pi/4 & 0.5 & 0.5 \end{bmatrix}$. While the spatial response in the direction of the additional targets is relatively low, there are significant sidelobes in other directions, suggesting that the resulting array may not be robust against unknown targets. Keep in mind that we apply a simple matched filter beamformer here, aimed at $(\theta, \phi) = (\frac{\pi}{2}, \frac{\pi}{4})$, to generate these spatial responses, and we perform no additional work to suppress the additional targets. We see that the results for (17) and the BA are very similar, which is somewhat expected since we see that they are very similar in Figs. 3 and 7. The sidelobe levels in our proposed method and the CRA in this example appear very similar, though they appear much closer to the mainlobe with the CRA. This shows us that, while they do share similarities, the sidelobe level and worst-case two-target CRB are distinct metrics since the CRA scores noticeably poorer in Fig. 8.

VI. CONCLUSIONS & DISCUSSION

In this work, we have proposed the use of a new metric for evaluating the performance of angle of arrival estimation: the worst-case two-target CRB. We have shown that this metric has similarities to the PSL metric, but since it is based on the CRB it is agnostic to the estimation method used, making it more broadly applicable. On the other hand, it mitigates another challenge typical of CRB-based methods, having to know the parameters of interest, by considering a worst-case for two targets at any two locations in space.

We have derived a method of optimizing a sensor selection based on the worst-case two-target CRB by relaxing the optimization problem to an SDP, which is solvable using off-the-shelf solvers. We show examples of selection results from applying the new metric and our proposed method and compare it to other sparse array designs. Without explicitly optimizing for sidelobe levels, we find that we still get reduced peak sidelobe levels when using our method compared to other CRB-based methods.

However, since our method only considers two targets, we can give no reconstruction or identifiability guarantees. These are important considerations that are taken in works on sparse array design and, as such, are worth investigating in conjunction with our proposed metric, i.e., to solve the array selection problem for a worst-case scenario, given that at least K targets should be identifiable, or given that the full candidate array must be reconstructable.

Besides this, we consider a number of other avenues of future work as well. Primarily, we want to investigate multiple-input and multiple-output (MIMO) systems. As discussed in Section I, sensor selection on transmit and receive can offer some key benefits to a MIMO system. For example, when the selections on transmit and receive are mutually exclusive, they can be used at the same time, potentially using continuous wave. Furthermore, on transmit, the sensors have to deal with far higher signal powers than on receive. Because of this, mitigating self-interference is important for transmission but not so much for reception. Including such considerations in optimizing the selections could lead to new optimal MIMO radar array designs.

Furthermore, we want to drop Assumption 1 to include the possibility of non-orthogonal target signals. This will produce a tighter CRB in terms of predicting estimator performance for cases where complete orthogonality cannot be guaranteed. This includes the active radar case, where multiple targets reflect the same waveform, and their relative Doppler shift, RCS fluctuations, and delay are insufficient to make the received waveforms orthogonal.

We also made the assumption that the targets exist in the far-field and can hence be described by a single DoA. While this assumption generally holds for monostatic long-range radar, it may not always hold for distributed radar systems and relatively close-range radar systems such as those found in vehicular applications, where the aperture or baseline of the array that is used is not that much smaller than the target ranges.

While we have restricted ourselves in this work to only consider binary selections, one could also optimize the gain of the selected sensors. This would relate the sensor selection problem to the spatial windowing practice. When employing spatial windowing, the gains of the sensors are adjusted individually in order to achieve specific mainlobe properties and sidelobe patterns. To incorporate this in the proposed method, we would need to use a more strict surrogate for the sparsity of the selection vector than the l_1-norm, and investigate how exactly we can relate the desired mainlobe properties and sidelobe patterns from spatial windowing to our CRB-based method.

Last, consider a multitask system, where the sensors that are not selected for the surveillance radar task are used for another task, such as communications and/or tracking radar. The metric we proposed here is especially relevant to the surveillance task. However, for example in the tracking task, as we have briefly discussed in Section IV-A, more information is available to use in the optimization, and as such may lead to different selections. By performing the sensor selection for multiple tasks, under the constraint that there is no overlap between the selections, we may find Pareto-optimal solutions to this multi-objective problem based on the importance of the different tasks. These solutions would then enable arrays to be used for multiple tasks without the need for time scheduling of the tasks while minimizing the performance loss of each of the tasks.

APPENDIX A
PROOF OF THEOREM 1

As specified in Section III, the unknown parameter vector is

$$\boldsymbol{\eta} = \begin{bmatrix} \mathrm{Re}\left[\boldsymbol{s}^{\mathsf{T}}\right] & \mathrm{Im}\left[\boldsymbol{s}^{\mathsf{T}}\right] & \boldsymbol{\omega}^{\mathsf{T}} \end{bmatrix}^{\mathsf{T}}.$$

For the derivation of the CRB, we start with the case where $T = 1$. The CRBM is given by the inverse of the Fisher information matrix (FIM) and the elements of the FIM for the data model given in (3), under the assumptions given in Section II and $T = 1$, are given by [43, Section 15.7]

$$[\mathcal{I}(\boldsymbol{\eta})]_{ij} = \frac{2}{\sigma^2} \operatorname{Re}\left[\frac{\partial \boldsymbol{s}^{\mathsf{H}}\boldsymbol{A}^{\mathsf{H}}}{\partial [\boldsymbol{\eta}]_i} \frac{\partial \boldsymbol{A}\boldsymbol{s}}{\partial [\boldsymbol{\eta}]_j}\right].$$

The following partial derivatives are required

$$\frac{\partial \boldsymbol{A}\boldsymbol{s}}{\partial \boldsymbol{\omega}_k} = s_k \boldsymbol{D}_k \in \mathbb{C}^{N\times 3}, \tag{18}$$

$$\frac{\partial \boldsymbol{A}\boldsymbol{s}}{\partial \boldsymbol{\omega}} = \boldsymbol{D} \circ (\boldsymbol{s}^{\mathsf{T}} \otimes \boldsymbol{J}_{N\times 3}) \in \mathbb{C}^{N\times 3K}, \tag{19}$$

$$\left[\frac{\partial \boldsymbol{A}\boldsymbol{s}}{\partial \operatorname{Re}[s_k]} \quad \frac{\partial \boldsymbol{A}\boldsymbol{s}}{\partial \operatorname{Im}[s_k]}\right] = \boldsymbol{a}_k \begin{bmatrix} 1 & \mathrm{j}\end{bmatrix} \in \mathbb{C}^{N\times 2}, \tag{20}$$

$$\left[\frac{\partial \boldsymbol{A}\boldsymbol{s}}{\partial \operatorname{Re}[\boldsymbol{s}]} \quad \frac{\partial \boldsymbol{A}\boldsymbol{s}}{\partial \operatorname{Im}[\boldsymbol{s}]}\right] = \begin{bmatrix} 1 & \mathrm{j}\end{bmatrix} \otimes \boldsymbol{A} \in \mathbb{C}^{N\times 2K}, \tag{21}$$

where $\boldsymbol{J}_{N\times M}$ is an $N \times M$ matrix of all ones. Before we can continue with the derivation of the entries of the FIM, we need the following proposition.

Proposition 2: Given an L-length vector $\boldsymbol{a}$, and an $N \times LM$ matrix $\boldsymbol{B}$ of $N \times M$ blocks, the matrix $\boldsymbol{C}$ given by

$$\boldsymbol{C} = \boldsymbol{B} \circ (\boldsymbol{a}^{\mathsf{H}} \otimes \boldsymbol{J}_{N\times M}),$$

has the property

$$\boldsymbol{C}^{\mathsf{H}}\boldsymbol{D}\boldsymbol{C} = \boldsymbol{B}^{\mathsf{H}}\boldsymbol{D}\boldsymbol{B} \circ (\boldsymbol{a}\boldsymbol{a}^{\mathsf{H}} \otimes \boldsymbol{J}_M),$$

where $\boldsymbol{D} \in \mathbb{C}^{N\times N}$.

Proof: First, the matrix $\boldsymbol{C}$ is partitioned as

$$\boldsymbol{C} = \begin{bmatrix} a_1^*\boldsymbol{B}_1 & a_2^*\boldsymbol{B}_2 & a_3^*\boldsymbol{B}_3 & \cdots & a_L^*\boldsymbol{B}_L\end{bmatrix},$$

where $(\cdot)^*$ denotes complex conjugation, a_l is the lth element of $\boldsymbol{a}$, and $\boldsymbol{B}_l$ is the lth $N \times M$ block of $\boldsymbol{B}$. Then,

$$\begin{aligned}\boldsymbol{D}\boldsymbol{C} &= \boldsymbol{D}(\boldsymbol{B} \circ (\boldsymbol{a}^{\mathsf{H}} \otimes \boldsymbol{J}_{N\times M})),\\ &= \begin{bmatrix} a_1^*\boldsymbol{D}\boldsymbol{B}_1 & a_2^*\boldsymbol{D}\boldsymbol{B}_2 & a_3^*\boldsymbol{D}\boldsymbol{B}_3 & \cdots & a_L^*\boldsymbol{D}\boldsymbol{B}_L\end{bmatrix},\\ &= \boldsymbol{D}\boldsymbol{B} \circ (\boldsymbol{a}^{\mathsf{H}} \otimes \boldsymbol{J}_{N\times M}).\end{aligned}$$

Since $\boldsymbol{C}^{\mathsf{H}}$ and $\boldsymbol{D}\boldsymbol{C}$ have conformable partitions, we may write

$$\begin{aligned}\boldsymbol{C}^{\mathsf{H}}\boldsymbol{D}\boldsymbol{C} &= \begin{bmatrix} a_1a_1^*\boldsymbol{B}_1^{\mathsf{H}}\boldsymbol{D}\boldsymbol{B}_1 & a_1a_2^*\boldsymbol{B}_1^{\mathsf{H}}\boldsymbol{D}\boldsymbol{B}_2 & \cdots\\ a_2a_1^*\boldsymbol{B}_2^{\mathsf{H}}\boldsymbol{D}\boldsymbol{B}_1 & a_2a_2^*\boldsymbol{B}_2^{\mathsf{H}}\boldsymbol{D}\boldsymbol{B}_2 & \cdots\\ \vdots & \vdots & \ddots\end{bmatrix},\\ &= \boldsymbol{B}^{\mathsf{H}}\boldsymbol{D}\boldsymbol{B} \circ (\boldsymbol{a}\boldsymbol{a}^{\mathsf{H}} \otimes \boldsymbol{J}_M).\end{aligned}$$

Using (18) to (21), and Proposition 2, we can set up the following nine blocks of the FIM:

$$\operatorname{Re}\left[\frac{\partial \boldsymbol{s}^{\mathsf{H}}\boldsymbol{A}^{\mathsf{H}}}{\partial \boldsymbol{\omega}^{\mathsf{T}}} \frac{\partial \boldsymbol{A}\boldsymbol{s}}{\partial \boldsymbol{\omega}}\right] = \mathcal{I}_{\boldsymbol{\omega}\boldsymbol{\omega}} = \operatorname{Re}\left[\boldsymbol{D}^{\mathsf{H}}\boldsymbol{D} \circ (\boldsymbol{s}\boldsymbol{s}^{\mathsf{H}} \otimes \boldsymbol{J}_3)\right],$$

$$\operatorname{Re}\left[\frac{\partial \boldsymbol{s}^{\mathsf{H}}\boldsymbol{A}^{\mathsf{H}}}{\partial \operatorname{Re}[\boldsymbol{s}^{\mathsf{T}}]} \frac{\partial \boldsymbol{A}\boldsymbol{s}}{\partial \operatorname{Re}[\boldsymbol{s}]}\right] = \mathcal{I}_{\mathrm{RR}} = \operatorname{Re}\left[\boldsymbol{A}^{\mathsf{H}}\boldsymbol{A}\right],$$

$$\operatorname{Re}\left[\frac{\partial \boldsymbol{s}^{\mathsf{H}}\boldsymbol{A}^{\mathsf{H}}}{\partial \operatorname{Im}[\boldsymbol{s}^{\mathsf{T}}]} \frac{\partial \boldsymbol{A}\boldsymbol{s}}{\partial \operatorname{Im}[\boldsymbol{s}]}\right] = \mathcal{I}_{\mathrm{RR}},$$

$$\operatorname{Re}\left[\frac{\partial \boldsymbol{s}^{\mathsf{H}}\boldsymbol{A}^{\mathsf{H}}}{\partial \operatorname{Im}[\boldsymbol{s}^{\mathsf{T}}]} \frac{\partial \boldsymbol{A}\boldsymbol{s}}{\partial \operatorname{Re}[\boldsymbol{s}]}\right] = \mathcal{I}_{\mathrm{IR}} = \operatorname{Im}\left[\boldsymbol{A}^{\mathsf{H}}\boldsymbol{A}\right],$$

$$\operatorname{Re}\left[\frac{\partial \boldsymbol{s}^{\mathsf{H}}\boldsymbol{A}^{\mathsf{H}}}{\partial \operatorname{Re}[\boldsymbol{s}^{\mathsf{T}}]} \frac{\partial \boldsymbol{A}\boldsymbol{s}}{\partial \boldsymbol{\omega}}\right] = \mathcal{I}_{\mathrm{R}\boldsymbol{\omega}} = \operatorname{Re}\left[\boldsymbol{A}^{\mathsf{H}}\boldsymbol{D} \circ (\boldsymbol{s}^{\mathsf{T}} \otimes \boldsymbol{J}_{N\times 3})\right],$$

$$\operatorname{Re}\left[\frac{\partial \boldsymbol{s}^{\mathsf{H}}\boldsymbol{A}^{\mathsf{H}}}{\partial \operatorname{Im}[\boldsymbol{s}^{\mathsf{T}}]} \frac{\partial \boldsymbol{A}\boldsymbol{s}}{\partial \boldsymbol{\omega}}\right] = \mathcal{I}_{\mathrm{I}\boldsymbol{\omega}} = \operatorname{Im}\left[\boldsymbol{A}^{\mathsf{H}}\boldsymbol{D} \circ (\boldsymbol{s}^{\mathsf{T}} \otimes \boldsymbol{J}_{N\times 3})\right].$$

To obtain the block of the CRBM corresponding to the DoA variance bounds, we use the Schur complement [38, A.5.5] to blockwise invert $\mathcal{I}(\boldsymbol{\eta})$:

$$\begin{aligned}&\mathrm{CRB}^{-1}_{\boldsymbol{\omega}\boldsymbol{\omega}}(\boldsymbol{\Omega})\\ &= \frac{2}{\sigma^2}\left(\mathcal{I}_{\boldsymbol{\omega}\boldsymbol{\omega}} - \begin{bmatrix}\mathcal{I}_{\mathrm{R}\boldsymbol{\omega}}\\ -\mathcal{I}_{\mathrm{I}\boldsymbol{\omega}}\end{bmatrix}^{\mathsf{T}}\begin{bmatrix}\mathcal{I}_{\mathrm{RR}} & -\mathcal{I}_{\mathrm{IR}}\\ \mathcal{I}_{\mathrm{IR}} & \mathcal{I}_{\mathrm{RR}}\end{bmatrix}^{-1}\begin{bmatrix}\mathcal{I}_{\mathrm{R}\boldsymbol{\omega}}\\ \mathcal{I}_{\mathrm{I}\boldsymbol{\omega}}\end{bmatrix}\right).\end{aligned}$$

By using [32, Appendix E], we can replace

$$\begin{aligned}&\begin{bmatrix}\mathcal{I}_{\mathrm{R}\boldsymbol{\omega}}\\ -\mathcal{I}_{\mathrm{I}\boldsymbol{\omega}}\end{bmatrix}^{\mathsf{T}}\begin{bmatrix}\mathcal{I}_{\mathrm{RR}} & -\mathcal{I}_{\mathrm{IR}}\\ \mathcal{I}_{\mathrm{IR}} & \mathcal{I}_{\mathrm{RR}}\end{bmatrix}^{-1}\begin{bmatrix}\mathcal{I}_{\mathrm{R}\boldsymbol{\omega}}\\ \mathcal{I}_{\mathrm{I}\boldsymbol{\omega}}\end{bmatrix}\\ &= \operatorname{Re}\left[(\mathcal{I}_{\mathrm{R}\boldsymbol{\omega}} + \mathrm{j}\mathcal{I}_{\mathrm{I}\boldsymbol{\omega}})^{\mathsf{H}}(\mathcal{I}_{\mathrm{RR}} + \mathrm{j}\mathcal{I}_{\mathrm{IR}})^{-1}(\mathcal{I}_{\mathrm{R}\boldsymbol{\omega}} + \mathrm{j}\mathcal{I}_{\mathrm{I}\boldsymbol{\omega}})\right],\end{aligned}$$

where, using re, using Proposition 2 again, we obtain

$$\begin{aligned}&(\mathcal{I}_{\mathrm{R}\boldsymbol{\omega}} + \mathrm{j}\mathcal{I}_{\mathrm{I}\boldsymbol{\omega}})^{\mathsf{H}}(\mathcal{I}_{\mathrm{RR}} + \mathrm{j}\mathcal{I}_{\mathrm{IR}})^{-1}(\mathcal{I}_{\mathrm{R}\boldsymbol{\omega}} + \mathrm{j}\mathcal{I}_{\mathrm{I}\boldsymbol{\omega}})\\ &= (\boldsymbol{D}^{\mathsf{H}}\boldsymbol{A}(\boldsymbol{A}^{\mathsf{H}}\boldsymbol{A})^{-1}\boldsymbol{A}^{\mathsf{H}}\boldsymbol{D}) \circ (\boldsymbol{s}^*\boldsymbol{s}^{\mathsf{T}} \otimes \boldsymbol{J}_3),\end{aligned}$$

which finally allows us to write

$$\begin{aligned}&\mathrm{CRB}^{-1}_{\boldsymbol{\omega}\boldsymbol{\omega}}(\boldsymbol{\Omega})\\ &= \frac{2}{\sigma_e^2}\operatorname{Re}\left[\boldsymbol{D}^{\mathsf{H}}(\boldsymbol{I} - \boldsymbol{A}(\boldsymbol{A}^{\mathsf{H}}\boldsymbol{A})^{-1}\boldsymbol{A}^{\mathsf{H}})\boldsymbol{D} \circ (\boldsymbol{s}^*\boldsymbol{s}^{\mathsf{T}} \otimes \boldsymbol{J}_3)\right].\end{aligned}$$

Recall that we assumed for simplicity that $T = 1$. To get the final result that completes the proof, we use the fact that the FIM of multiple independent identically distributed (i.i.d.) snapshots is the sum of the FIMs of the individual snapshots [32, Appendix F]. Summing the snapshots we get

$$\begin{aligned}&\mathrm{CRB}^{-1}_{\boldsymbol{\omega}\boldsymbol{\omega}}(\boldsymbol{\Omega})\\ &= \frac{2}{\sigma_e^2}\operatorname{Re}\left[\boldsymbol{D}^{\mathsf{H}}(\boldsymbol{I} - \boldsymbol{A}(\boldsymbol{A}^{\mathsf{H}}\boldsymbol{A})^{-1}\boldsymbol{A}^{\mathsf{H}})\boldsymbol{D} \circ (\boldsymbol{S}^{\mathsf{H}}\boldsymbol{S} \otimes \boldsymbol{J}_3)\right].\end{aligned}$$

which simplifies to (8). This expression is of course similar to the CRB as presented in [32], but we would like to call attention to the specific structure of the $\boldsymbol{D}$ and $\boldsymbol{S}^{\mathsf{H}}\boldsymbol{S} \otimes \boldsymbol{J}_3$ matrices, which have a particular structure due to the DoAs of the targets being described by vectors instead of scalars.

APPENDIX B
PROOF OF PROPOSITION 1

Since we assumed $\boldsymbol{R}$ to be diagonal, we know the CRB will be a block diagonal matrix. Neglecting the constant factors, we write the selection dependent EFIM for angle of arrival estimation of the kth target as

$$\begin{aligned}&\boldsymbol{F}_k(\Delta\boldsymbol{\omega},\boldsymbol{p})\\&=\mathrm{Re}\left[\boldsymbol{D}_k^{\mathsf{H}}\boldsymbol{P}\boldsymbol{D}_k-\boldsymbol{D}_k^{\mathsf{H}}\boldsymbol{P}\boldsymbol{A}\left(\boldsymbol{A}^{\mathsf{H}}\boldsymbol{P}\boldsymbol{A}\right)^{-1}\boldsymbol{A}^{\mathsf{H}}\boldsymbol{P}\boldsymbol{D}_k\right]\\&=\mathrm{Re}[\ddot{\boldsymbol{Z}}(\boldsymbol{p})-\dot{\boldsymbol{Z}}_k^{\mathsf{H}}(\Delta\boldsymbol{\omega},\boldsymbol{p})\boldsymbol{Z}^{-1}(\Delta\boldsymbol{\omega},\boldsymbol{p})\dot{\boldsymbol{Z}}_k(\Delta\boldsymbol{\omega},\boldsymbol{p})]\,.\end{aligned}$$

Let us evaluate the three distinct terms of the EFIM individually. We then obtain

$$\boldsymbol{Z}(\Delta\boldsymbol{\omega},\boldsymbol{p})=\sum_{n=1}^{N}p_n\begin{bmatrix}1&\exp[\mathrm{j}\boldsymbol{x}_n^{\mathsf{T}}\Delta\boldsymbol{\omega}]\\\exp[-\mathrm{j}\boldsymbol{x}_n^{\mathsf{T}}\Delta\boldsymbol{\omega}]&1\end{bmatrix}, \tag{22}$$

$$\begin{aligned}\dot{\boldsymbol{Z}}_1(\Delta\boldsymbol{\omega},\boldsymbol{p})&=\dot{\boldsymbol{Z}}(\Delta\boldsymbol{\omega},\boldsymbol{p})\\&=\sum_{n=1}^{N}p_n\begin{bmatrix}1\\\exp[-\mathrm{j}\boldsymbol{x}_n^{\mathsf{T}}\Delta\boldsymbol{\omega}]\end{bmatrix}\boldsymbol{x}_n^{\mathsf{T}}\,,\end{aligned} \tag{23}$$

$$\begin{aligned}\dot{\boldsymbol{Z}}_2(\Delta\boldsymbol{\omega},\boldsymbol{p})&=\boldsymbol{Q}\dot{\boldsymbol{Z}}^{*}(\Delta\boldsymbol{\omega},\boldsymbol{p})\\&=\sum_{n=1}^{N}p_n\begin{bmatrix}\exp[\mathrm{j}\boldsymbol{x}_n^{\mathsf{T}}\Delta\boldsymbol{\omega}]\\1\end{bmatrix}\boldsymbol{x}_n^{\mathsf{T}}\,,\\\ddot{\boldsymbol{Z}}(\boldsymbol{p})&=\sum_{n=1}^{N}p_n\boldsymbol{x}_n\boldsymbol{x}_n^{\mathsf{T}}\,,\end{aligned} \tag{24}$$

where $\boldsymbol{Q}=\left[\begin{smallmatrix}0&1\\1&0\end{smallmatrix}\right]$. We see that $\ddot{\boldsymbol{Z}}(\boldsymbol{p})$ does not depend on $\boldsymbol{\Omega}$ at all, while $\boldsymbol{Z}(\Delta\boldsymbol{\omega},\boldsymbol{p})$ and $\dot{\boldsymbol{Z}}_k(\Delta\boldsymbol{\omega},\boldsymbol{p})$ only depend on the difference of the columns of $\boldsymbol{\Omega}$, $\Delta\boldsymbol{\omega}$. Additionally, $\boldsymbol{Z}(\Delta\boldsymbol{\omega},\boldsymbol{p})$ and $\dot{\boldsymbol{Z}}(\boldsymbol{p})$ do not depend on the target.

Furthermore, we can show that $\boldsymbol{Z}(\Delta\boldsymbol{\omega},\boldsymbol{p})$ and $\dot{\boldsymbol{Z}}_k(\Delta\boldsymbol{\omega},\boldsymbol{p})$ have some symmetries in k and $\Delta\boldsymbol{\omega}$, namely

$$\dot{\boldsymbol{Z}}_k(\Delta\boldsymbol{\omega},\boldsymbol{p})=\dot{\boldsymbol{Z}}_k^{*}(-\Delta\boldsymbol{\omega},\boldsymbol{p})\,, \tag{25}$$

$$\boldsymbol{Z}(\Delta\boldsymbol{\omega},\boldsymbol{p})=\boldsymbol{Z}^{*}(-\Delta\boldsymbol{\omega},\boldsymbol{p})\,, \tag{26}$$

$$\begin{aligned}\boldsymbol{Z}^{\mathsf{T}}(\Delta\boldsymbol{\omega},\boldsymbol{p})&=\boldsymbol{Q}\boldsymbol{Z}(\Delta\boldsymbol{\omega},\boldsymbol{p})\boldsymbol{Q}\\&=\boldsymbol{Z}^{*}(\Delta\boldsymbol{\omega},\boldsymbol{p})\,.\end{aligned} \tag{27}$$

Using (25) to (27) we can derive the following two symmetries for the EFIM:

$$\boldsymbol{F}_k(\Delta\boldsymbol{\omega},\boldsymbol{p})=\boldsymbol{F}_k(-\Delta\boldsymbol{\omega},\boldsymbol{p})\,,\quad \boldsymbol{F}_1(\Delta\boldsymbol{\omega},\boldsymbol{p})=\boldsymbol{F}_2(\Delta\boldsymbol{\omega},\boldsymbol{p})\,,$$

since

$$\begin{aligned}&\mathrm{Re}\left[\dot{\boldsymbol{Z}}_k^{\mathsf{H}}(\Delta\boldsymbol{\omega},\boldsymbol{p})\boldsymbol{Z}^{-1}(\Delta\boldsymbol{\omega},\boldsymbol{p})\dot{\boldsymbol{Z}}_k(\Delta\boldsymbol{\omega},\boldsymbol{p})\right]\\&=\mathrm{Re}\left[\dot{\boldsymbol{Z}}_k^{\mathsf{T}}(-\Delta\boldsymbol{\omega},\boldsymbol{p})(\boldsymbol{Z}^{*}(-\Delta\boldsymbol{\omega},\boldsymbol{p}))^{-1}\dot{\boldsymbol{Z}}_k^{*}(-\Delta\boldsymbol{\omega},\boldsymbol{p})\right]\\&=\mathrm{Re}\left[(\dot{\boldsymbol{Z}}_k^{\mathsf{H}}(-\Delta\boldsymbol{\omega},\boldsymbol{p})\boldsymbol{Z}^{-1}(-\Delta\boldsymbol{\omega},\boldsymbol{p})\dot{\boldsymbol{Z}}_k(-\Delta\boldsymbol{\omega},\boldsymbol{p}))^{*}\right]\\&=\mathrm{Re}\left[\dot{\boldsymbol{Z}}_k^{\mathsf{H}}(-\Delta\boldsymbol{\omega},\boldsymbol{p})\boldsymbol{Z}^{-1}(-\Delta\boldsymbol{\omega},\boldsymbol{p})\dot{\boldsymbol{Z}}_k(-\Delta\boldsymbol{\omega},\boldsymbol{p})\right],\end{aligned}$$

and

$$\begin{aligned}&\mathrm{Re}\left[\dot{\boldsymbol{Z}}_2^{\mathsf{H}}(\Delta\boldsymbol{\omega},\boldsymbol{p})\boldsymbol{Z}^{-1}(\Delta\boldsymbol{\omega},\boldsymbol{p})\dot{\boldsymbol{Z}}_2(\Delta\boldsymbol{\omega},\boldsymbol{p})\right]\\&=\mathrm{Re}\left[\dot{\boldsymbol{Z}}^{\mathsf{T}}(\Delta\boldsymbol{\omega},\boldsymbol{p})\boldsymbol{Q}(\boldsymbol{Q}\boldsymbol{Z}^{*}(\Delta\boldsymbol{\omega},\boldsymbol{p})\boldsymbol{Q})^{-1}\boldsymbol{Q}\dot{\boldsymbol{Z}}^{*}(\Delta\boldsymbol{\omega},\boldsymbol{p})\right]\\&=\mathrm{Re}\left[\dot{\boldsymbol{Z}}^{\mathsf{T}}(\Delta\boldsymbol{\omega},\boldsymbol{p})(\boldsymbol{Z}^{*}(\Delta\boldsymbol{\omega},\boldsymbol{p}))^{-1}\dot{\boldsymbol{Z}}^{*}(\Delta\boldsymbol{\omega},\boldsymbol{p})\right]\\&=\mathrm{Re}\left[\dot{\boldsymbol{Z}}_1^{\mathsf{H}}(\Delta\boldsymbol{\omega},\boldsymbol{p})\boldsymbol{Z}^{-1}(\Delta\boldsymbol{\omega},\boldsymbol{p})\dot{\boldsymbol{Z}}_1(\Delta\boldsymbol{\omega},\boldsymbol{p})\right],\end{aligned}$$

where we used the fact that $\boldsymbol{Q}=\boldsymbol{Q}^{-1}$ and that the order of the matrix inverse and transpose is interchangeable.

Finally, note the $\ddot{\boldsymbol{Z}}(\boldsymbol{p})$ is real-valued and the product

$$\dot{\boldsymbol{Z}}_k^{\mathsf{H}}(\Delta\boldsymbol{\omega},\boldsymbol{p})\boldsymbol{Z}^{-1}(\Delta\boldsymbol{\omega},\boldsymbol{p})\dot{\boldsymbol{Z}}_k(\Delta\boldsymbol{\omega},\boldsymbol{p})\in\mathbb{R}^{3\times3}\,,$$

as well, so $\boldsymbol{F}_k(\Delta\boldsymbol{\omega},\boldsymbol{p})$ is real-valued as well.

APPENDIX C
CONVEX RELAXATIONS OF (14)

To relax (14), we use the following consequence of the Schur complement[38, A.5.5]:

$$\text{if}\boldsymbol{A}\succ\boldsymbol{0},\text{ then}$$

$$\begin{bmatrix}\boldsymbol{A}&\boldsymbol{B}\\\boldsymbol{B}^{\mathsf{H}}&\boldsymbol{C}\end{bmatrix}\succeq0\iff\boldsymbol{C}-\boldsymbol{B}^{\mathsf{H}}\boldsymbol{A}^{-1}\boldsymbol{B}\succeq0\,. \tag{28}$$

Let us take the second constraint in (14) and reformulate it using (28):

$$\begin{aligned}&\boldsymbol{F}(\Delta\boldsymbol{\omega},\tilde{\boldsymbol{p}})\succeq\boldsymbol{C}^{-1}\,,\ \forall\Delta\boldsymbol{\omega}\in\mathcal{D}_+\\&\qquad\Updownarrow\text{ if }\quad\boldsymbol{F}(\Delta\boldsymbol{\omega},\tilde{\boldsymbol{p}})\succ\boldsymbol{0}\\&\begin{bmatrix}\boldsymbol{F}(\Delta\boldsymbol{\omega},\tilde{\boldsymbol{p}})&\boldsymbol{I}\\\boldsymbol{I}&\boldsymbol{C}\end{bmatrix}\succeq\boldsymbol{0}\,,\ \forall\Delta\boldsymbol{\omega}\in\mathcal{D}_+\,.\end{aligned} \tag{29}$$

Note that $\boldsymbol{F}(\Delta\boldsymbol{\omega},\tilde{\boldsymbol{p}})$ is positive definite (PD) when we have $M\geq K$ and the sensor positions are diverse enough (span all dimensions). To obtain LMIs, we introduce another auxiliary variable, $\boldsymbol{G}$, which we use to bound the part of $\boldsymbol{F}(\Delta\boldsymbol{\omega},\tilde{\boldsymbol{p}})$ that depends on $\Delta\boldsymbol{\omega}$:

$$\ddot{\boldsymbol{Z}}(\boldsymbol{p})-\boldsymbol{G}\succeq\boldsymbol{F}(\Delta\boldsymbol{\omega},\tilde{\boldsymbol{p}})\,,$$

which is equivalent to

$$\boldsymbol{G}-\dot{\boldsymbol{Z}}^{\mathsf{H}}(\Delta\boldsymbol{\omega},\boldsymbol{p})\boldsymbol{Z}^{-1}(\Delta\boldsymbol{\omega},\boldsymbol{p})\dot{\boldsymbol{Z}}(\Delta\boldsymbol{\omega},\boldsymbol{p})\succeq\boldsymbol{0}\,.$$

Through another application of the Schur complement, we can turn this and (29) into

$$\begin{bmatrix}\ddot{\boldsymbol{Z}}(\boldsymbol{p})-\boldsymbol{G}&\boldsymbol{I}\\\boldsymbol{I}&\boldsymbol{C}\end{bmatrix}\succeq\boldsymbol{0}\,,$$

$$\begin{bmatrix}\boldsymbol{G}&\dot{\boldsymbol{Z}}^{\mathsf{H}}(\Delta\boldsymbol{\omega},\boldsymbol{p})\\\dot{\boldsymbol{Z}}(\Delta\boldsymbol{\omega},\boldsymbol{p})&\boldsymbol{Z}(\Delta\boldsymbol{\omega},\boldsymbol{p})\end{bmatrix}\succeq\boldsymbol{0}\,,\ \forall\Delta\boldsymbol{\omega}\in\mathcal{D}_+\,,$$

giving us the LMI constraints with which we can construct the convex SDP in (15). Here we do require that $\boldsymbol{Z}(\Delta\boldsymbol{\omega}, \boldsymbol{p})$ is PD for all $\Delta\boldsymbol{\omega}$ in $\mathcal{D}_+$, which should be taken care of in the construction of $\mathcal{D}_+$. The matrix $\boldsymbol{Z}(\Delta\boldsymbol{\omega}, \boldsymbol{p})$ is positive semidefinite (PSD) for all $\Delta\boldsymbol{\omega}$ and invertible for $|\Delta\boldsymbol{\omega}| \neq 0$, but ill-conditioned for small $|\Delta\boldsymbol{\omega}|$.

REFERENCES

[1] A. Molisch and M. Win, "MIMO systems with antenna selection," *IEEE Microw. Mag.*, vol. 5, no. 1, pp. 46–56, Mar. 2004.

[2] H. Wang, K. Yao, G. Pottie, and D. Estrin, "Entropy-based sensor selection heuristic for target localization," in *Proc. 3rd Int. Symp. Inf. Process. Sens. Netw.*, Berkeley, CA, USA: ACM, Apr. 2004, pp. 36–45.

[3] X. Wang, E. Aboutanios, M. Trinkle, and M. G. Amin, "Reconfigurable adaptive array beamforming by antenna selection," *IEEE Trans. Signal Process.*, vol. 62, no. 9, pp. 2385–2396, May 2014.

[4] I. Gupta and A. Ksienski, "Effect of mutual coupling on the performance of adaptive arrays," *IEEE Trans. Antennas Propag.*, vol. AP-31, no. 5, pp. 785–791, Sep. 1983.

[5] B. Friedlander and A. Weiss, "Direction finding in the presence of mutual coupling," *IEEE Trans. Antennas Propag.*, vol. 39, no. 3, pp. 273–284, Mar. 1991.

[6] E. BouDaher, F. Ahmad, M. G. Amin, and A. Hoorfar, "Mutual coupling effect and compensation in non-uniform arrays for direction-of-arrival estimation," *Digit. Signal Process.*, vol. 61, pp. 3–14, Feb. 2017.

[7] R. Rajamaki and V. Koivunen, "Sparse active rectangular array with few closely spaced elements," *IEEE Signal Process. Lett.*, vol. 25, no. 12, pp. 1820–1824, Dec. 2018.

[8] M. Robinson and R. Ghrist, "Topological localization via signals of opportunity," *IEEE Trans. Signal Process.*, vol. 60, no. 5, pp. 2362–2373, May 2012.

[9] A. Moffet, "Minimum-redundancy linear arrays," *IEEE Trans. Antennas Propag.*, vol. AP-16, no. 2, pp. 172–175, Mar. 1968.

[10] R. N. Bracewell, *Radio Astronomy Techniques*. Berlin, Heidelberg: Springer, 1962.

[11] C.-H. Jang, F. Hu, F. He, J. Li, and D. Zhu, "Low-redundancy large linear arrays synthesis for aperture synthesis radiometers using particle swarm optimization," *IEEE Trans. Antennas Propag.*, vol. 64, no. 6, pp. 2179–2188, Jun. 2016.

[12] K. Blanton and J. McClellan, "New search algorithm for minimum redundancy linear arrays," in *Proc. ICASSP 1991 Int. Conf. Acoust. Speech Signal Process.*, Apr. 1991, vol. 2, pp. 1361–1364.

[13] J. Dong, Q. Li, R. Jin, Y. Zhu, Q. Huang, and L. Gui, "A method for seeking low-redundancy large linear arrays in aperture synthesis microwave radiometers," *IEEE Trans. Antennas Propag.*, vol. 58, no. 6, pp. 1913–1921, Jun. 2010.

[14] R. Kozick and S. Kassam, "Linear imaging with sensor arrays on convex polygonal boundaries," *IEEE Trans. Syst. Man Cybern.*, vol. 21, no. 5, pp. 1155–1166, Sep./Oct. 1991.

[15] R. Kozick and S. Kassam, "Synthetic aperture pulse-echo imaging with rectangular boundary arrays (acoustic imaging)," *IEEE Trans. Image Process.*, vol. 2, no. 1, pp. 68–79, Jan. 1993.

[16] J. Kohonen, V. Koivunen, and R. Rajamäki, "Planar additive bases for rectangles," Nov. 2017, *arXiv:1711.08812*.

[17] P. Pal and P. P. Vaidyanathan, "Nested arrays: A novel approach to array processing with enhanced degrees of freedom," *IEEE Trans. Signal Process.*, vol. 58, no. 8, pp. 4167–4181, Aug. 2010.

[18] J. He, L. Li, and T. Shu, "2-D direction finding using parallel nested arrays with full co-array aperture extension," *Signal Process.*, vol. 178, 2021, Art. no. 107795. [Online]. Available: https://www.sciencedirect.com/science/article/pii/S016516842030339X

[19] P. P. Vaidyanathan and P. Pal, "Sparse sensing with co-prime samplers and arrays," *IEEE Trans. Signal Process.*, vol. 59, no. 2, pp. 573–586, Feb. 2011.

[20] Q. Wu, F. Sun, P. Lan, G. Ding, and X. Zhang, "Two-dimensional direction-of-arrival estimation for co-prime planar arrays: A partial spectral search approach," *IEEE Sensors J.*, vol. 16, no. 14, pp. 5660–5670, Jul. 2016.

[21] S. Shahsavari, J. Millhiser, and P. Pal, "Fundamental trade-offs in noisy super-resolution with synthetic apertures," in *Proc. ICASSP 2021 IEEE Int. Conf. Acoust. Speech Signal Process.*, Jun. 2021, pp. 4620–4624.

[22] C.-L. Liu and P. P. Vaidyanathan, "Cramér–Rao bounds for coprime and other sparse arrays, which find more sources than sensors," *Digit. Signal Process.*, vol. 61, pp. 43–61, Feb. 2017.

[23] S. Joshi and S. Boyd, "Sensor selection via convex optimization," *IEEE Trans. Signal Process.*, vol. 57, no. 2, pp. 451–462, Feb. 2009.

[24] F. Athley, "Optimization of element positions for direction finding with sparse arrays," in *Proc. 11th IEEE Signal Process. Workshop Stat. Signal Process.*, Aug. 2001, pp. 516–519.

[25] A. Gershman and J. Bohme, "A note on most favorable array geometries for DOA estimation and array interpolation," *IEEE Signal Process. Lett.*, vol. 4, no. 8, pp. 232–235, Aug. 1997.

[26] H. Gazzah and S. Marcos, "Cramer-Rao bounds for antenna array design," *IEEE Trans. Signal Process.*, vol. 54, no. 1, pp. 336–345, Jan. 2006.

[27] H. Gazzah and J. P. Delmas, "CRB-Based design of linear antenna arrays for near-field source localization," *IEEE Trans. Antennas Propag.*, vol. 62, no. 4, pp. 1965–1974, Apr. 2014.

[28] V. Roy, S. P. Chepuri, and G. Leus, "Sparsity-enforcing sensor selection for DOA estimation," in *Proc. 5th IEEE Int. Workshop Comput. Adv. Multi-Sens. Adapt. Process.*, St. Martin, France: IEEE, Dec. 2013, pp. 340–343.

[29] S. P. Chepuri and G. Leus, "Sparsity-promoting sensor selection for non-linear measurement models," *IEEE Trans. Signal Process.*, vol. 63, no. 3, pp. 684–698, Feb. 2015.

[30] E. Tohidi, M. Coutino, S. P. Chepuri, H. Behroozi, M. M. Nayebi, and G. Leus, "Sparse antenna and pulse placement for colocated MIMO radar," *IEEE Trans. Signal Process.*, vol. 67, no. 3, pp. 579–593, Feb. 2019.

[31] L. Vandenberghe and S. Boyd, "Semidefinite programming," *SIAM Rev.*, vol. 38, no. 1, pp. 49–95, Mar. 1996.

[32] P. Stoica and A. Nehorai, "MUSIC, maximum likelihood, and cramer-rao bound," *IEEE Trans. Acoust. Speech Signal Process.*, vol. 37, no. 5, pp. 720–741, May 1989.

[33] A. Dogandzic and A. Nehorai, "Cramer-Rao bounds for estimating range, velocity, and direction with an active array," *IEEE Trans. Signal Process.*, vol. 49, no. 6, pp. 1122–1137, Jun. 2001.

[34] U. Baysal and R. Moses, "On the geometry of isotropic arrays," *IEEE Trans. Signal Process.*, vol. 51, no. 6, pp. 1469–1478, Jun. 2003.

[35] C. A. Kokke, M. Coutino, L. Anitori, R. Heusdens, and G. Leus, "Sensor selection for angle of arrival estimation based on the two-target cramér-rao bound," in *Proc. ICASSP 2023 IEEE Int. Conf. Acoust. Speech Signal Process.*, Jun. 2023, pp. 1–5.

[36] C. A. Kokke, M. Coutino, R. Heusdens, and G. Leus, "Array design based on the worst-case Cramér-Rao bound to account for multiple targets," in *Proc. 57th Asilomar Conf. Signals Syst. Comput.*, Oct. 2023, pp. 1174–1178.

[37] A. Arora, B. S. Mysore R., and B. Ottersten, "Cramer-Rao bound on DOA estimation of finite bandwidth signals using a moving sensor," in *Proc. ICASSP 2020 IEEE Int. Conf. Acoust. Speech Signal Process.*, May 2020, pp. 4697–4701.

[38] S. P. Boyd and L. Vandenberghe, *Convex Optimization*. Cambridge, U.K.: Cambridge Univ. Press, 2004.

[39] J. Li, L. Xu, P. Stoica, K. W. Forsythe, and D. W. Bliss, "Range compression and waveform optimization for MIMO radar: A Cramér–Rao bound based study," *IEEE Trans. Signal Process.*, vol. 56, no. 1, pp. 218–232, Jan. 2008.

[40] S. Diamond and S. Boyd, "CVXPY: A python-embedded modeling language for convex optimization," *J. Mach. Learn. Res.*, vol. 17, pp. 1–5, 2016. [Online]. Available: https://stanford.edu/boyd/papers/pdf/cvxpy_paper.pdf

[41] M. Andersen, J. Dahl, and L. Vandenberghe, "CVXOPT: A Python package for convex optimization, version 1.3.2," 2023. [Online]. Available: https://cvxopt.org

[42] Á. González, "Measurement of areas on a sphere using fibonacci and latitude–longitude lattices," *Math. Geosci.*, vol. 42, no. 1, pp. 49–64, Jan. 2010.

[43] S. Kay, *Fundamentals of Statistical Signal Processing, Volume I: Estimation Theory (Prentice Hall Signal Processing Series)*, 1st ed., Englewood Cliffs, NJ, USA: Pearson, Apr. 1993.

COSTAS A. KOKKE (Graduate Student Member, IEEE) received the M.Sc. degree in electrical engineering from Delft University of Technology, Delft, The Netherlands, in 2018. Between 2018 and starting the Ph.D. project in 2021, he worked with the Electronic Defence department of the Netherlands Organisation for Applied Scientific Research as a junior scientist working on disruptive signal processing for communications. His Ph.D. research is mainly on optimization of sparse radar arrays and is a collaboration project between the Radar Technology department of the Netherlands Organisation for Applied Scientific Research, the Netherlands Defence Academy, and the Signal Processing Systems group of Delft University of Technology.

MARIO COUTINO (Member, IEEE) received the M.Sc. and Ph.D. degrees (cum laude) in electrical engineering from the Delft University of Technology, Delft, The Netherlands, in 2016 and 2021, respectively. Since 2020, he has been with TNO, The Netherlands, as a Signal Processing Researcher working on radar and sonar. He held positions with Thales Netherlands in 2015, and Bang & Olufsen during 2015 to 2016. He was a Visiting Researcher with RIKEN AIP and the Digital Technological Center, University of Minnesota, in 2018 and 2019, respectively. His research interests include array signal processing, signal processing on networks, submodular and convex optimization, and numerical linear algebra. He was the recipient of the Best Student Paper Award for his publication with the CAMSAP 2017 conference in Curacao and IEEE Signal Processing Society 2023 Best Ph.D. Dissertation Award.

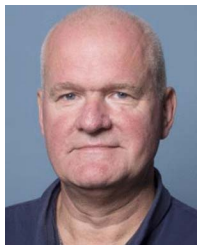

RICHARD HEUSDENS (Senior Member, IEEE) received the M.Sc. and Ph.D. degrees from the Delft University of Technology, Delft, The Netherlands, in 1992 and 1997, respectively. In 1992, he joined the Digital Signal Processing Group with Philips Research Laboratories, Eindhoven, The Netherlands. He has worked on various topics in the field of signal processing, such as image/video compression and VLSI architectures for image processing algorithms. In 1997, he joined the Circuits and Systems Group of Delft University of Technology, where he was also a Postdoctoral Researcher. In 2000, he moved to the Information and Communication Theory (ICT) Group, where he became an Assistant Professor responsible for the audio/speech signal processing activities within the ICT group. Since 2002, he has been an Associate Professor in the Faculty of Electrical Engineering, Mathematics and Computer Science, Delft University of Technology. He held visiting positions with KTH (Royal Institute of Technology, Sweden) in 2002 and 2008 and was a Guest Professor with Aalborg University from 2014 to 2016. Since 2019, he has been a Full Professor with the Netherlands Defence Academy, Den Helder, The Netherlands. He is involved in research projects that cover subjects such as audio and acoustic signal processing, sensor signal processing, distributed optimization, and security/privacy.

GEERT LEUS (Fellow, IEEE) received the M.Sc. and Ph.D. degree in electrical engineering from the KU Leuven, Leuven, Belgium, in June 1996 and May 2000, respectively. He is currently a Full Professor with the Faculty of Electrical Engineering, Mathematics and Computer Science of the Delft University of Technology, The Netherlands. He was the recipient of the 2021 EURASIP Individual Technical Achievement Award, 2005 IEEE Signal Processing Society Best Paper Award, and 2002 IEEE Signal Processing Society Young Author Best Paper Award. He is a Fellow of EURASIP. He was a Member-at-Large of the Board of Governors of the IEEE Signal Processing Society, the Chair of the IEEE SIGNAL PROCESSING FOR COMMUNICATIONS and Networking Technical Committee, the Chair of the EURASIP Technical Area Committee on Signal Processing for Multisensor Systems, the Editor-in-Chief of the *EURASIP Journal on Advances in Signal Processing* and the Editor-in-Chief of *EURASIP Signal Processing.*